SHOCKWAVE INTERACTIONS WITH ARGON GLOW DISCHARGES

THESIS

Nicholas S. Siefert, Lieutenant, USAF

AFIT/GAP/ENP/06-18

DEPARTMENT OF THE AIR FORCE
AIR UNIVERSITY

AIR FORCE INSTITUTE OF TECHNOLOGY

Wright-Patterson Air Force Base, Ohio

AFIT/GAP/ENP/06-18

SHOCKWAVE INTERACTIONS WITH ARGON GLOW DISCHARGES

THESIS

Presented to the Faculty

Department of Engineering Physics

Graduate School of Engineering and Management

Air Force Institute of Technology

Air University

Air Education and Training Command

in Partial Fulfillment of the Requirements for the

Degree of Master of Science (Applied Physics)

Nicholas S. Siefert, BS,

Lieutenant, USAF

March 2006

AFIT/GAP/ENP/06-18

SHOCKWAVE INTERACTIONS WITH ARGON GLOW DISCHARGES

Nicholas S. Siefert, BS
Lieutenant, USAF

Approved:

William F. Bailey (Chairman)	Date

Biswa N. Ganguly (Member)	date

Glen P. Perram (Member)	date

AFIT/GAP/ENP/06-18

Abstract

Shockwaves, generated by a spark gap, were launched into a direct current gas discharge in argon. The modification of the positive column structure was characterized using a microwave hairpin resonator, a diode laser, photo-deflection, floating probes and optical fibers. The data collected with a microwave hairpin resonator showed a ratio of electron number density across a Mach 1.5 shock front of 2.1 and a ratio across a Mach 1.8 shock front of 2.7. These electron number density ratios were nearly the same in both the active discharge and in the afterglow. The corresponding neutral density ratios, given by the Rankine-Hougoniot relationship, are 1.7 and 2.0. These measurements suggest that non-equilibrium electrons can be compressed at shock fronts in weakly-ionized gases, even though the electron thermal velocity is two orders of magnitude greater than the shock velocity.

Using the hairpin resonator, in combination with photo-deflection and optical fibers, established the relative location of the peak in electron density with respect to the neutral particle shock front. The location of the peak of the electron number density was displaced behind the neutral particle shock front. At Mach 1.5, the electron number density peaked 25 mm behind the shock front in the active discharge and 50 mm behind the shock front in the afterglow.

The density of excited $1s_5$ metastable states across the shock front was measured using diode laser absorption spectroscopy. In theory, excited state atoms can be compressed at a shock front only if the lifetime of the excited state is longer than the time

to transit though the shock front. Across Mach 1.8 shock fronts, the measured ratio of the metastable state density was 2.5, but the predicted value from the Rankine-Hougoniet relationship was only 2.0. Data collected over a range of different Mach numbers showed the same general trend as the predicted values, but were consistently greater than predicted.

A region of space-charge separation, termed a double layer, at the shock front is set up due to the diffusion of mobile electrons from the post-shock region into the pre-shock region. The voltage of the double layer at the shock front was measured and compared with previous numerical results by Jaffrin [1] and Adamovich et al. [2]. In order to compare with previous research, the double layer potential was divided by the electron temperature. The measured potential was nearly always one and a half times greater than the potential calculated by Jaffrin [1] and over two times greater than the value calculated by Adamovich et al. [2].

Data collected suggests that the light emission enhancement seen by previous researchers [3,4] is not due to an electron-accelerating double layer, but rather due to the compression of metastable states and electrons at the shock front.

Acknowledgments

I thank my wife for all her support throughout the Master's degree. I thank the Dayton Area Graduate Studies Institute for the funds to attend AFIT part-time. I thank Drs. Biswa Ganguly and Peter Bletzinger for conceiving of the design of for the shock tube experiment. I thank Professor Bailey for his helpful comments, criticism and suggestions throughout the writing process. I thank my parents for leaving all of those math and physics books lying around at home. I thank Brian Sands for his help with the diode laser experiment and the hairpin resonator experiment. Finally, I thank Drs. Glen Perram and Robert Leiweke for their help with diode laser absorption theory.

Nicholas S. Siefert

Table of Contents

List of Figures

List of Tables

SHOCKWAVE INTERACTIONS WITH ARGON GLOW DISCHARGES

I. Introduction

Relevance of Topic

At a shock front in weakly-ionized gases, there is a region of net space-charge separation whose characteristic length is the electron Debye length. The electron Debye length is a measure of the length of non-neutrality that plasma can support. One of the definitions of a plasma is that there is quasi-neutrality, i.e. there are approximately the same number of positively and negatively charged species. Quasi-neutrality is valid only when the electron Debye length is much smaller than the characteristic length of the plasma.

At a shock front, the characteristic length is the shock front thickness. Under typical glow discharge conditions, the shock thickness and the electron Debye length are the same order of magnitude. Therefore, quasi-neutrality is not a valid assumption at a shock front in glow discharges. In experiments where the electron Debye length is comparable to the shock thickness, an enhancement in optical light emission has been reported at the shock front [3,4].

This thesis will address the following questions: what is the cause of the optical emission enhancement at the shock front? Is it possible to compress electrons at a shock front whose mean energy is ~5 eV? What is the potential (voltage) of the double layer at the shock front? The results in this thesis strongly suggest the following answers to these questions. First, the light enhancement can be explained by the compression of electrons and metastable states at the shock front. Second, electrons with a mean energy of ~5 eV can be compressed by a shockwave. Third, within experimental error, the potential of this double layer matches with the Jaffrin theory if one replaces the equilibrium electron

temperature in the theory with the non-equilibrium electron temperature typical of glow discharges.

Shockwave Basics

Before addressing the topic of shockwave interaction with weakly-ionized gas, the jump conditions for the neutral species at a shock front in argon are presented. The following equations are the ratio of pressures before and after the shock front, the ratio of densities and the ratio of temperatures.[1]

$$\frac{p_2}{p_1} = 1 + 1.25\left(M^2 - 1\right) \tag{1}$$

$$\frac{\rho_2}{\rho_1} = \frac{4M^2}{M^2 + 3} \tag{2}$$

$$\frac{T_2}{T_1} = \frac{p_2}{p_1}\frac{\rho_1}{\rho_2} = \frac{\left[1 + 1.25\left(M^2 - 1\right)\right]\left(M^2 + 3\right)}{4M^2} \tag{3}$$

where 1 = before shock front, 2 = after shock front, p = pressure, ρ = density, T = temperature and M = upstream Mach number. Figure 1 shows that the ratios of pressure, density and temperature across a shock front increase as a function of the upstream Mach number. The pressure ratio is equal to the density ratio times the temperature ratio.

[1] Eqs. (1), (2) and (3) are valid for noble gases, such as argon, where the ratio of specific heats, γ, is 5/3.
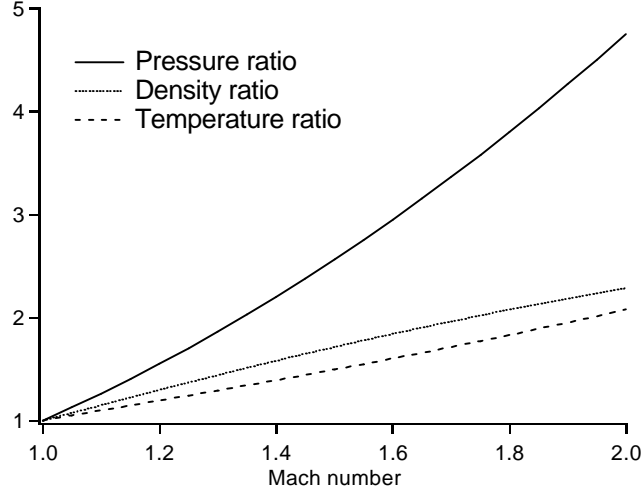
Figure 1: Pressure, Density and Temperature Ratios across a Shock Front versus Upstream Mach number

The Mach number for most shockwave in this thesis is 2, which corresponds to a temperature ratio of 2.1, a density ratio of 2.3 and a pressure ratio of 4.8.

Shockwave Interaction with Weakly-Ionized Gases

At the shock front in weakly-ionized gases, large density gradients and highly mobile electrons create conditions that are favorable for the diffusion of the electrons with respect to the positive ions. Diffusion in weakly-ionized gases is substantially different from diffusion in neutral gases. Under conditions of quasi-neutrality, the smallest change in the relative concentration of the electrons and ions leads to the creation of a region of net space-charge, i.e. to polarization of the plasma accompanied by the creation of the a strong electric field. This electric field prevents further polarization and inhibits the diffusion of electrons. The electrons and the ions diffuse together and this is called ambipolar diffusion. Early analytic attempts by Jafrin [1] to determine the charge separation and self-consistent electric field generation at shock fronts in weakly ionized plasma (ionization fraction, $\alpha = 10^{-3}$) assumed that the electron

3

and ion temperatures were equal and assumed that the electron Debye length was much smaller than the shock thickness. Under these assumptions, quasi-neutrality holds. The predicted electric fields at the shock front were quite large; however, since the Debye length was quite small, the potential difference was only roughly $ln(\rho_2/\rho_1)kT_e/e$, where ρ_2/ρ_1 is the ratio of density behind the shock front to the density before the shock front, kTe is the electron temperature and e is the electric charge. An analysis for the case of partially and fully ionized argon is presented in Greenberg et al. [5] and Lieberman et al. [6].[2] An analysis for the case of shockwaves in weakly-ionized plasma is also presented in Zel'dovich et al. [7]. Figure 2 shows the net space-charge, the electric field and the potential at the shock front, found in Zel-dovich et al. [7]. Note that the there is a positive potential jump across the shock front.
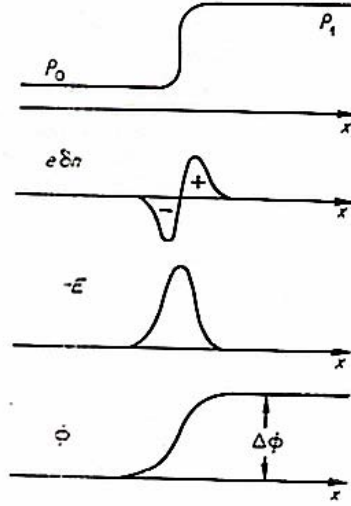
Figure 2: Mass Density, ρ , Space Charge Density, $e\ \delta n$, Electric Field, $-E$, and Electric Potential, Φ, Distributions at the Shock Front in Weakly-Ionized Gases

---

[2] In the case of fully-ionized plasma, the Mach number is no longer the speed of the shockwave divided by the speed of sound. Instead, the Mach number is the speed of the shockwave divided by the ion-acoustic speed.

In the shock reference frame, the electric field in Jaffrin [1] is an ambipolar electric field that inhibits the electrons from diffusing out of the shock front. Ambipolar diffusion only holds when the characteristic length of diffusion is greater than ten times the Debye length [8,9]. Diffusion to the walls of a positive column, when the Debye length is 0.3 mm and the radius of the tube is 15 mm, is another example of ambipolar diffusion.[3] Under ambipolar diffusion, the electrons can not freely diffuse to the walls of the discharge because they are pulled back by the slower moving ions. Since Jaffrin [1] assumed that the shock thickness is fifty times greater than the Debye length, the electric field at the shock front is also an example of an ideal ambipolar field. In both of the last two examples, the ambipolar electric field inhibits the free diffusion of electrons due to a gradient of electron number density. The gradient of density is created in positive column because electrons are created near the center of the tube and are lost at the wall. The gradient of density is created at the shock front because charged species are compressed at the shock front like the neutral species. The ambipolar field acts as an efficient way for the electrons to transfer their kinetic energy to the ions [10] because the ambipolar electric field decelerates the light, mobile electrons. Since the electrons set up the double layer potential, their mean energy should slightly decrease across the shock front.

There are three assumptions made by Jaffrin [1] that are not valid for shockwaves under my experimental conditions. First, Jaffrin [1] assumed that the electron Debye length is fifty times less than the shock front thickness. Experimentally, both the electron Debye length and the shock front thickness are roughly 0.5 mm. The assumption of ambipolar diffusion at the shock front, therefore, does not hold. Second, Jaffrin [1] assumed that the electron temperature before the shock front was equal to the positive ion temperature, which is equal to the neutral gas temperature. However, the electron temperature (~50,000 K) is much greater than the ion temperature both in front of (300 K) and behind the shock front (400 K - 600 K, depending on Mach number). Third,

---

[3] Characteristic diffusion length = radius / first zero of Bessel's function = 15 mm / 2.4 = 6.25 mm > 10

Debye length = 10*(0.3 mm) = 3 mm

Characteristic diffusion length / Debye length ~ 20 for diffusion to the walls of the positive column

Jaffrin [1] assumed that the electrons have no drift velocity. This assumption is valid only in the afterglow of a discharge. In an active discharge, electrons have a drift velocity that is greater than the shockwave velocity. This drift velocity can affect the fluxes of charged particles entering and leaving the shock front. Besides these three assumptions not holding, there is another difference between Jaffrin's conditions and experimental conditions. In Jaffrin's numerical calculations, the ionization fraction was 10^{-3}. The ionization fraction in a typical glow discharge is 10^{-7}, i.e. one electron for every ten million neutral argon atoms.

The numerical discharge-shockwave code by Adamovich et al. [2] provides a more realistic simulation than the work by Jaffrin [1]. Adamovich et al. [2] assumed that the electron temperature could be much greater than the gas temperature. They did not have to assume quasi-neutrality because they treated the electrons and positive ions as separate particles and because they used a Poisson Equation solver to calculate the charge-separation, electric field and double layer potential at the shock front. As well as charged particle species, their code calculated the increase in argon excited metastable states at the shock front. They published results at the following discharge condition: 10 Torr Argon, Mach 2, T_e = 3.6 eV. Figure 3 shows the data under these conditions.
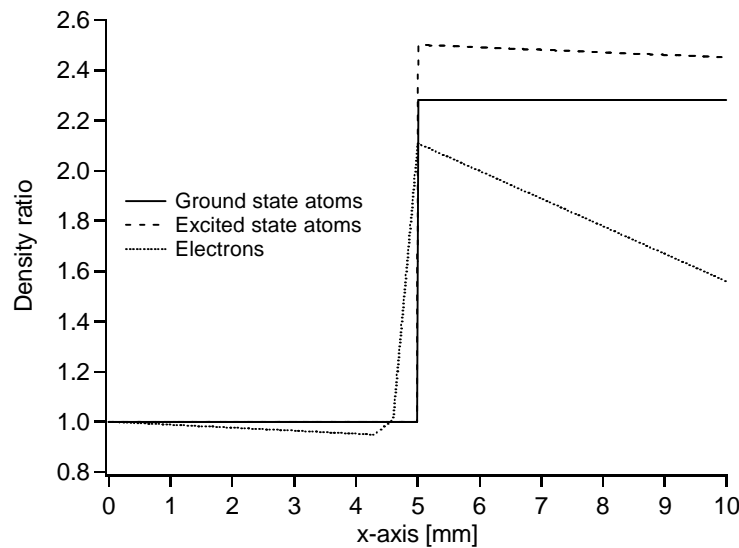
Figure 3: Calculated Species Densities across the Shock Front

6

Here are some noticeable features of Figure 3: a) there is an increase in both the electron number density and the excited species density at the shock front; b) there is a 5% dip in the electron number density before the shock front; c) the electron density decays after the shock front; and d) the excited state species are compressed 10% more than the ground state atoms and the electrons are compressed 10% less than the ground state atoms. The reason for the 10% more/less is not mentioned in the text of the paper. The results from Figure 3 will be used later in this thesis to compare with the experimental results.

Using the numerical predictions from Adamovich et al. [2], the optical light enhancement seen by Bletzinger et al. [4] can be explained by the increase in electron number density and metastable state density at the shock front. What can't be explained by previous analytic and numerical studies are the results by Bletzinger et al. [4] showing that the strength of the light emission enhancement and the strength of the electron number density enhancement at the shock front was polarization dependent, i.e. the strength of the enhancement depended on whether the shock traveled from the anode to the cathode or from the cathode to the anode. This means that the drift velocity of the electrons in the discharge was in the direction of the shock velocity for one case and the drift velocity was in the opposite direction for another case. In later work [11], they measured an enhancement in the discharge current by ten percent as a weak shock passed through a glow discharge from cathode to anode, but no rise in current was detected in the anode to cathode case. The increase in global current is particularly important because it suggests that electrons are being produced at the shock front, not just being compressed. There will be no attempt in this thesis to explain the increase in global discharge current, but there will be an effort in Analysis Section IV to explain the polarization dependence of the light emission and the electron number density enhancement.

Previous work by Siefert et al. [3] found experimental evidence for optical light enhancement at the shock front in the afterglow of a nitrogen glow discharge. The experiments were conducted in the afterglow of a 0.75 Torr nitrogen positive column, meaning that the discharge was switched off before the arrival of the shockwave at the

location of the optical detectors. Therefore, the energy for the emission enhancement could not have come directly from the power supply. The strength of the emission enhancement was observed to increase linearly with increasing Mach number and to decrease exponentially with increasing time in the afterglow. They concluded that the energy to create the enhancement in optical light emission came from the shockwave via a strong electron accelerating double layer. The results in this thesis and the numerical simulation by Adamovich et al [2] in weakly-ionized argon raise serious questions about whether electrons can be accelerated at the shock front. The rapid emission enhancement reported by Siefert et al. [3] is probably not due to an electron acceleration double layer, but rather the light emission enhancement at the shock front is due to nitrogen specific effects involving the collision of two A $^3\Sigma_u^+$ metastable states.

Ionization Waves

The advantage of using argon rather than nitrogen as the background gas in this study is that the chemistry is more straightforward. Argon was chosen over other noble gases because its atomic weight is closest to the molecule weight of nitrogen. The disadvantage of using argon is that, for the range of pressures and current densities of interest, the argon glow discharge is stratified, i.e. there exists either standing or moving waves of ionization. In glow discharges, there are many types of ionization waves. Some are due to recombination instabilities; others are due to attachments instabilities. Reviews of ionization waves in glow discharges have been conducted by multiple authors, such Perarek [12], Olson et al. [13], Garscadden [14] and Raizer [15].[4] The ionization waves in

---

[4] These authors stress the importance of distinguishing between ion acoustic waves and ionization waves. The confusion between the two waves stems from the fact that the wavelengths and frequencies of the waves can be the same order of magnitude. Ion-acoustic waves only exist at pressures below 10 mTorr since these waves are damped by collisions with neutral species.

argon glow discharges at the pressures and currents relevant to this thesis are due to a two-step ionization instability associated with the presence of metastable states.[5]

At the conditions of interest for this thesis, the ionization waves appear as large amplitude fluctuations in light emission, metastable density, electric field and electron number density.[6] Experimentally, the waves travel from the anode to the cathode with velocities between 100 m/s and 300 m/s. H.S. Robertson [16] demonstrated with a numerical model that two-step ionization of metastable states leads to an instability. In his model, if there are only a small number of metastable states, then the plasma was found to be stable. For this reason, an argon glow discharge will be stable by keeping the current below a threshold or by adding a buffer gas mixture, e.g. roughly 3% nitrogen or oxygen, to quench the metastable states.

In this thesis, when a stable discharge is required, the discharge current is kept below the threshold current where the ionization waves begin. When a stable discharge is not required (or when an unstable discharge is preferred), the shockwaves are sent into a discharge whose electron number density and metastable density vary periodically in time. Appendix A reviews previous studies of ionization waves and also discusses the issue of chaos in ionization waves.

Double Layers

If electrons had no charge, but had the same mass and same non-equilibrium temperature, they could not be compressed at a shock front because they could not lose a substantial amount of momentum to the heavy particles.[7] However, electrons do carry charge, which means that they can lose momentum via an electric field. Positive ions can collide with neutral species and lose momentum, which means that their density can be

---

[5] Metastable states are excited states that can not radiate to the ground state via dipole selection rules.

[6] Measured by optical fibers, laser absorption, floating probes and microwave resonators, respectively.

[7] From the continuity equation, the particle velocity times the particle density is constant for each species. In order for the density to increase, the particle species must be able to lose directed velocity.

compressed. A region of space-charge separation at the shock front creates an electric field that takes momentum from the electrons, allowing them to be compressed. The generic term for such a region of charge separation in the volume of a plasma is a double layer. A double layer is a shock-like structure in the electrostatic potential that can be accompanied by steep gradients in electron temperature, charge particles number density and light emission [17,18,19]. Double layers consist of two adjacent charge layers of equal and opposite charge. Double layers differ from sheaths in that they are not connected to the plasma boundary. They may be current-carrying or current-free; they can be 1-D, 2-D or 3-D; they can be either transient or steady-state; and they can be in a magnetic field or without a magnetic field [20]. Some double layers accelerate electrons, such as the auroal double layers [21]; others accelerate positive ions [22].

The ambipolar double layer in Jaffrin [1] is similar to the double layer between two current-free, loss-less[8] plasmas with different electron temperatures. Ishiguro et al. [23] determined that, "The hot electrons spend their energy to create the double layer potential." The double layer prevents the two temperature regions from mixing at the speed of the hotter electrons. This is not quite intuitive. In the mixing of neutral gases with different temperatures, the atoms in the hot regions are allowed to freely diffuse into the cold region. This does not occur at the boundary between plasmas with two distinct temperatures because a region of net space-charge would quickly form, setting up an electric field. This ambipolar field impedes the diffusion of the hotter electrons into the colder plasma. The region forms because there are different fluxes of charged species passing through the boundary between the two plasmas. Since the double layer in this case takes energy from the electrons on the hot side, this type of double layer can not, by itself, explain the enhancement in light emission at the shock front seen by previous researchers. There is, however, another double layer with possible relevance to the shock front in 1-2 Torr argon glow discharges.

Williamson et al. [19] studied a 2-D double layer that formed at the abrupt transition between two tube diameters (2.6 cm to 0.6 cm) in a 1 Torr positive column in

---

[8] Loss-less = no sink or source for charged particles, i.e. no production or loss of charged particles

helium. The double layer existed in the volume of the plasma, not at the walls. Laser absorption techniques measured the He ($2\,^3S_1$) metastable density. This particular double layer was current-carrying and there was a polarization dependence, i.e. more excited species existed when the anode was placed inside the smaller section than when the anode was placed in the larger tube diameter. The double layer in Williamson et al. [19] is similar to the double layer shown in Figure 4, from Maciel et al. [24].
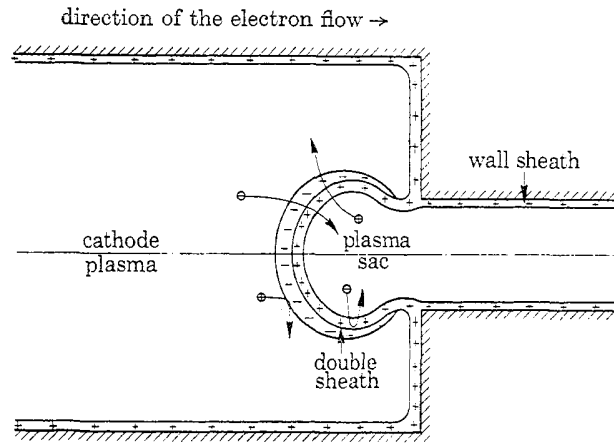
Figure 4: Schematic of Double Layer Formed at the Constriction of Discharge Radius

The electric field of the double layer added to the external electric field of the discharge when the anode was in the smaller section and subtracted from the external field when the cathode was in the smaller section. The reason for the polarization dependence was that the electrons only needed to gain energy when the anode was in the smaller section. The reduced electric field, *E/N*, at the double layer was greater than on either side. Polarization dependence is a characteristic of current-carrying double layers [24]. The light emission near a shock front in weakly-ionized gas nitrogen seen by Bletzinger et al. [4] resembles the light emission found by Williamson et al. [19] because in both cases there is a polarization dependence to the light emission. However, either way a shockwave travels into a discharge, the electrons should lose energy at the shock front. Whereas, in the Williamson et al. [19] experiment, the electrons gain energy at the double layer only when the anode was placed in the smaller section.

11

II. Experimental Set Up

Figure 5 shows a schematic of the experimental set up and Figure 6 is a picture of the laboratory. The experimental set up is broken down into the following main parts: DC glow discharge with two cylindrical electrodes; a co-axial spark gap for generating the shockwave; two He-Ne lasers for measuring the shock velocity; two optical fibers connected to photomultiplier tubes (PMTs) for measuring optical emission; two floating probes for measuring the double layer potential; a hairpin resonator for measuring the electron number density; and a diode laser for measuring metastable state density. Note: the diagnostics for measuring the electron number density and the metastable density are not shown in the schematic below.
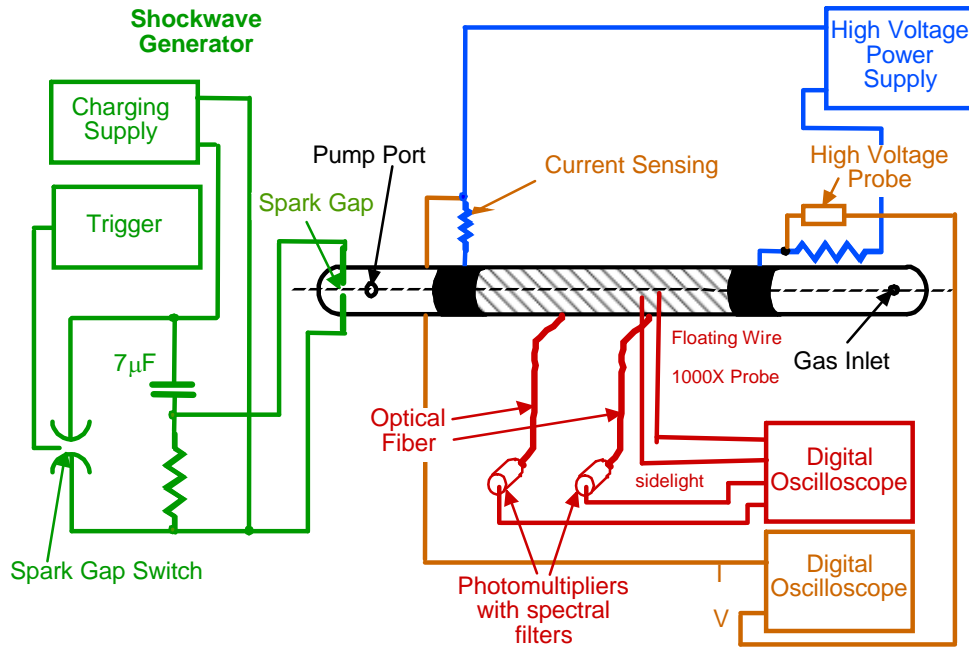
Figure 5: Schematic of Experiment
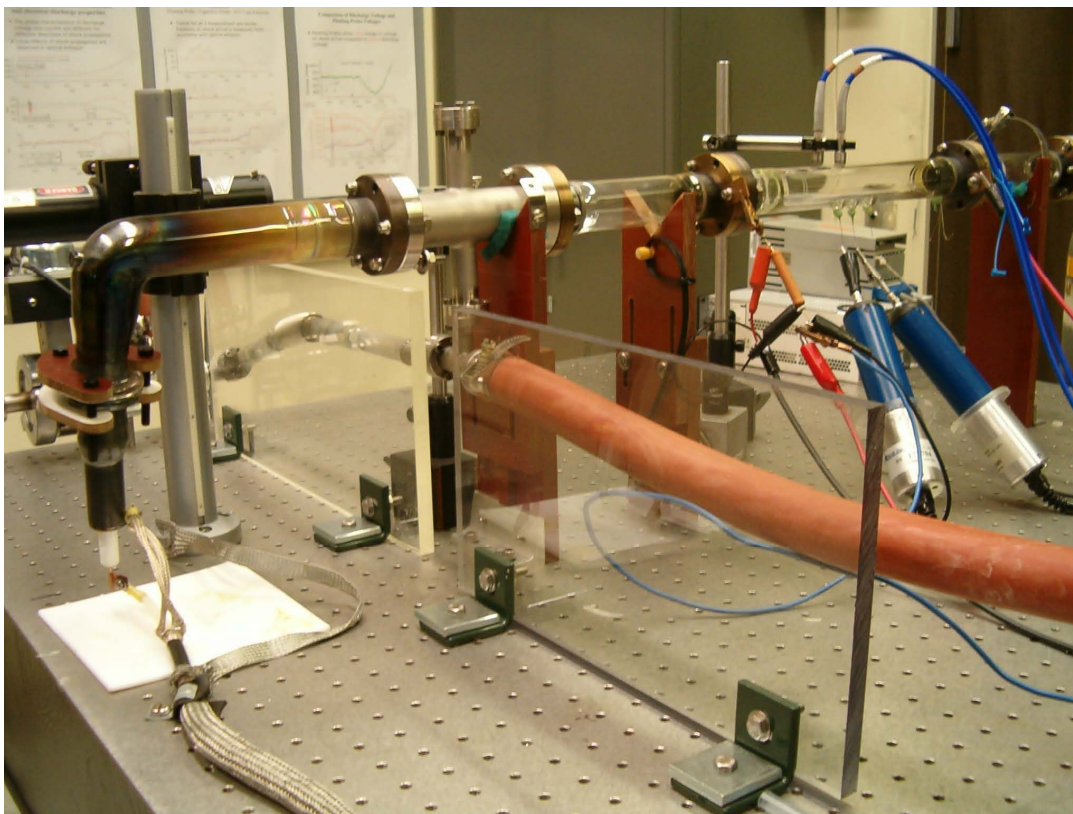
Figure 6: Apparatus

To the left in Figure 6 is the spark gap that creates the shockwave. Once created, the shockwave passes through the 90 degree bend in the tube and then passes through the discharge region. Note that the discharge is not running in this figure. Pictures of the discharge running are shown in Figure 7 and Figure 8.
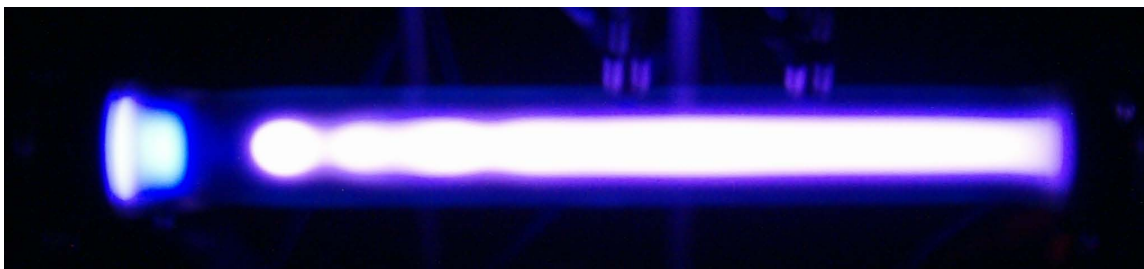
Figure 7: 0.33 Torr, 30 mA Argon Discharge

Figure 8: 1 Torr, 30 mA Argon Discharge

In the above figures, the cathode is located on the left side and the anode is located on the right side. The positive column is the glow that fills most of the discharge tube. There is a Faraday dark space between the cathode and the positive column. The Faraday Dark Space is larger at 0.33 Torr than at 1 Torr. At 0.33 Torr, there are noticeable standing striations at the beginning of the positive column. These striations are stationary ionization waves.

Shockwave Arrival, Light Emission and Floating Probe Diagnostics

All experiments were conducted on a Newport Research Series Table Top. The DC active discharge was created between two conformal wall electrodes made out of Kovar and spaced 30 cm apart. Kovar is an iron based alloy with nickel and cobalt, whose chemistry is closely controlled so as to result in low, uniform, thermal expansion so that it can be sealed to glass components. In the figures above, the cathode is at the left electrode and the anode is at the right electrode. The radius of the glass tube was 1.5 cm. The gas pressure of the system could be varied between 0.25 Torr and 2.0 Torr, and was monitored with a capacitance manometer. The current in the discharge could be varied between 0 and 30 mA, corresponding to a current density between 0 and 4.2 mA/cm^2.

Table 1: Summary of Discharge Parameters

Current (mA)	Radius (cm)	Length (cm)	Pressure (Torr)
0-30	1.5	30	0.25-2

Two floating wires placed inside the glass tube measured a voltage difference in the positive column. The wires were separated by 2 cm and were connected to 1000X, 100 MΩ high voltage probes. The voltage difference divided by the distance between the wires provided the time-dependent or steady-state axial electric field in the positive column. The typical values of *E/N* were 6 Td (1 Td = 1×10^{-17} V·cm^2). The difference between the plasma potential and the floating potential on the wires is the voltage drop in the sheath around the wire. The sheath voltage drop is proportional to the electron temperature. As long as the electron temperature does not vary across the positive column, the two wires can accurately measure the axial electric field in the positive column. The floating probes were also used to measure the potential of the double layer across the shock front. One difficulty here is that the electron temperature will vary across the shock front. Although, this change is expected to be roughly 10% based on the simulation by Adamovich et al. [2].

Two Helium-Neon laser beams were passed perpendicularly across the discharge to determine the arrival of the shockwave at the optical detectors and to determine the shockwave velocity. We used two Uniphase He-Ne lasers with an output of 10mW each. Each beam was directed onto a photodiode such that the photodiode signal jump was approximately proportional to the line-averaged density gradient jump [25]. This pulse determined the location of the shock front. The photodiodes were manufactured by ThorLabs and have a bandwidth of 100 MHz. The limit in the resolution of this diagnostic tool was not the response time of the detector, but rather the spatial width of the laser beam. The beam diameter was 2 mm, leading to a time resolution of 4 μs for a shock velocity of 500 m/s. In comparison, the neutral particle shock front dimension for these pressures is on the order of 1 mm. Deflection signals from two laser beams spaced 2 cm apart, measured the average shock velocity between the two laser locations.

To convert the shock velocity into a Mach number, it was necessary to determine the gas temperature inside the glow discharge. The temperature was estimated from the energy balance between the input power and the conductive heat loss to the walls. The mean temperature inside the discharge was calculated by solving for the transport of Joule heat via conduction to the walls, as detailed by Raizer [26]. For example, the

estimated mean temperature of a 2 Torr, 20 mA discharge was 320 K ± 5 K. The speed of sound in argon at 300 K is 319 m/s. Therefore, the mean speed of sound in the 2 Torr, 20 mA discharge was 329 ± 2 m/s.

The optical emission from the discharge was collected by two fibers, with collimating lens attached in front. The fibers were manufactured by OceanOptics and the collimating lens (F230SMA-B) were manufactured by Thor Lab. The collimating lens work for wavelengths between 600 and 1050 nm. The spatial resolution of the fibers with the collimating lens was 2 mm. The photons emitted from the positive column were collected by the fibers and sent to a PhotoMultipler Tube (PMT). The PMT was produced in-house and powered by a Stanford Research Instruments model PS 310/325 high voltage power supply. An Andover Corporation optical bandpass filter centered at 763 nm was placed just before the PMTs. The 763 nm filter only allowed the radiation from the $2p_6$ excited state to the $1s_5$ metastable to pass through. The radiative lifetime of this transition is 36.5 ns [32]. The radiative lifetime to the $1s_4$ state is 213 ns and the radiative lifetime to the $1s_2$ state is 169 ns [32]. The collision quenching time at 2 Torr is 223 ns [34]. This means that the effective loss time is 23 ns and the branching ratio from the excited $2p_6$ state to the $1s_5$ metastable is 64%. This effective loss time of 23 ns is an order of magnitude less than the time needed to pass through the shock front. The Rankine-Hougoniot relationship for compression at a shock front is only valid if the neutral species have a lifetime greater than the time to transit through the shock front. Therefore, excited $2p_6$ states can not be compressed at the shock front.

The shockwaves in this experiment were created inside a 2.7 cm diameter co-axial spark gap with an inner tungsten pin electrode. A power supply, produced in-house, charged up low-inductance capacitors that deposited up to 350 Joule of energy in less than 5 μs using an EG&G spark gap (GP-22B) switch and a EG&G trigger module (TM-11A.) The capacitance value was 7 μF. We used low-inductance capacitors in order to have a fast discharge. The voltage from the in-house power supply was varied from 5 kV to 12 kV. In this way, the shock velocity could be varied from 400 m/s to 700 m/s. We did not exceed 12 kV in order to inhibit the creation of UV and X-ray photons in the spark gap. The discharging of the capacitors into the co-axial spark gap was initiated by a

BNC Model 555 Pulse/Delay Generator. This master clock sent out timing signals to the EG&G spark gap/trigger module and to the external trigger inputs of the LeCroy oscilloscopes.

There was a ninety degree bend in the tube after the spark gap and before the discharge. The bend is not shown in the 2-D schematic in Figure 5, but can be seen in Figure 6. The bend slightly slowed down the shock. The purpose of the bend was to prevent the photons created by the spark gap from reaching the discharge.

Hairpin Resonator for Measuring Electron Number Density

A microwave hairpin resonator was used to measure the electron number density before, during and after the shock front. The hairpin consisted of a U-shaped piece of 0.5 mm diameter gold wire. The length of the hairpin was 24 mm and the width was 5 mm. Gold wire was chosen for its relatively large conductance. Figure 9 shows a diagram of the hairpin resonator system. Epoxy held the loop wire and the hairpin together without allowing an electrical connection. The oscillating currents from the sweep generator created oscillating magnetic fields in the loop wire. The oscillating magnetic fields coupled to the hairpin when the frequency from the sweep generator reached the hairpin's quarter-wave resonance. The hairpin radiated at the frequency of the sweep generator. A crystal detector at the end a waveguide outside of the discharge volume measures the microwave power radiated by the hairpin.
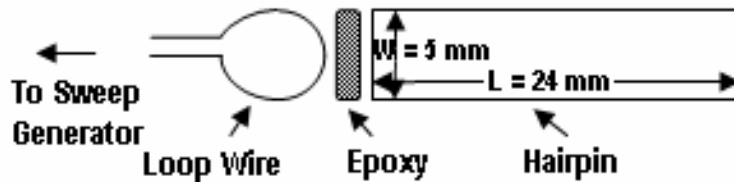
Figure 9: Hairpin Schematic

Figure 10 shows the location of the hairpin inside of the discharge. The hairpin resonator is the gold U-shaped device inside the glass tube. To the right is an X-band rectangular waveguide that detects the radiation from the hairpin.
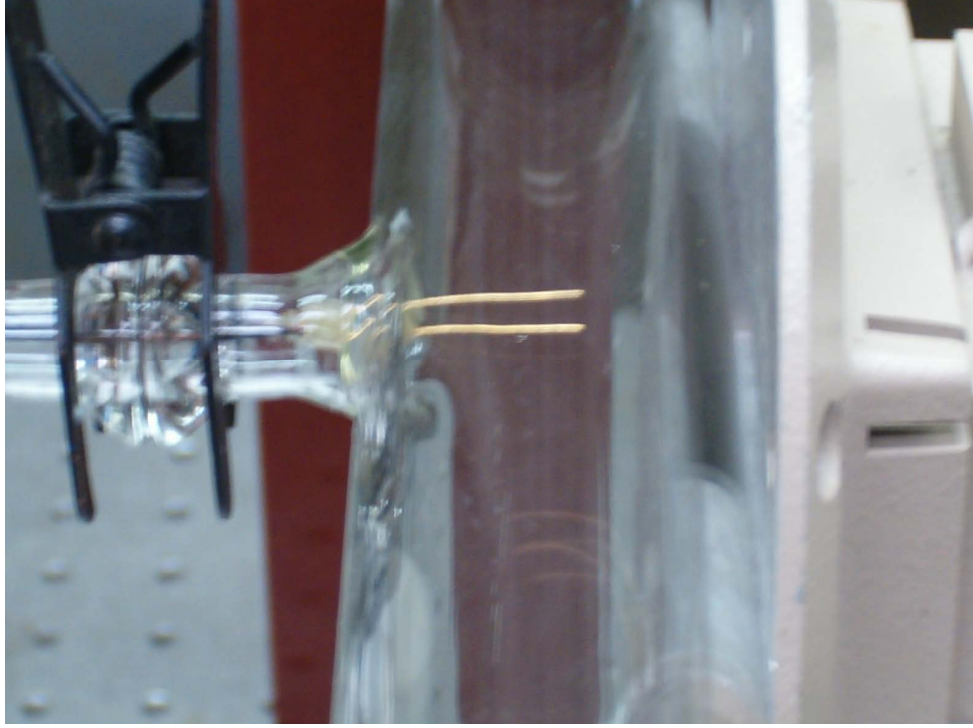
Figure 10: Hairpin Resonator inside of Discharge Tube

The peak resonant frequency of the hairpin [28] is

$$f_{resonant} = \frac{c}{4L\sqrt{\varepsilon}} \qquad , \qquad (4)$$

where c is the speed of light in a vaccum, L is the length of the hairpin, and ε is the dielectric constant of the medium between the hairpin wires. Since L equals 24 mm, the peak resonance in vacuum was 3.08 GHz. The quality factor Q in vacuum was 110. The dielectric constant in collisionless plasma can be expressed as

$$\varepsilon = 1 - \frac{\omega_p^{\,2}}{\omega^2} \quad , \tag{5}$$

where ω_p is the electron plasma frequency, such that $\omega_p^{\,2} = \frac{4\pi\, e^2 n_e}{m_e}$, and ω is the

microwave frequency in rad/s. By combining the last two equations and including a

sheath correction factor, Piejak et al. [28] expressed the electron number density as

$$n_e = \frac{f_{res}^{\,2} - f_0^{\,2}}{0.81 \cdot C_{sheath}} \quad , \tag{6}$$

where f_{res} is the resonant frequency with the plasma on and f_o is the resonant frequency
with the plasma off. The unit for the frequencies is GHz and the unit for n_e is 10^{10} cm^{-3}.
Piejak et al. [28] calculated the sheath correction factor, C_{sheath}, for the case of a
collisionless sheath. C_{sheath} is a function of both the radius of the wire, the width of the
hairpin and the electron Debye length. The details of the hairpin resonator for measuring
steady-state electron number density can be found in journal papers by Stenzel [27] and
Piejak et al. [28].

Elastic collisions between electrons and neutral argon atoms will affect the shape
of the resonance curve and the location of the peak frequency. In collisional plasma, the
dielectric constant is complex. For hairpin resonators, the real component of the dielectric
constant affects the peak resonance frequency and the imaginary component affects the
quality factor Q. The real component is $1 - [\omega_p^{\,2}/(v_{en}^{\,2} + \omega^2)]$. The imaginary component
is $(v_{en}/\omega)[\omega_p^{\,2}/(v_{en}^{\,2} + \omega^2)]$, which causes a decrease in Q proportional to $n_e \cdot v_{en}$. The
electron-neutral collision frequency is approximated in Raizer [15] to be $v_{en}/p = 5.3 \cdot 10^9$ s^{-1} Torr^{-1}, assuming a constant gas temperature and constant electron temperature. At a
pressure of 0.5 Torr argon, v_{en} is approximately 2.6×10^9 sec^{-1}, or $(v_{en}/\omega)^2 \sim 0.01$. For this
collision frequency, the correction to the real component of the dielectric constant is
negligible, validating the use of Equation (6). However, the imaginary component, which
represents collision absorption of the microwave power, affects the hairpin shape by

19

causing a decrease in the quality factor Q with increasing $n_e \cdot v_{en}$. The decrease in the quality factor of the resonance curves set an upper limit to $n_e \cdot v_{en}$, which is why data collected with the hairpin resonator was kept below 0.5 Torr. This requirement also limited the Mach number used in these experiments because both the gas density and electron number density increase at the shock front, which causes an increase $n_e \cdot v_{en}$ and decrease in Q.

In order to convert the hairpin resonator into a time-dependent diagnostic tool, resonance curves were built up at multiple points in time. From each resonance curve, the peak frequency was chosen and inserted into Eq (6) to determine the electron number density at that instant in time.

The virtue of the hairpin resonator compared to other microwave techniques [29] is the hairpin's axial spatial resolution, which for our hairpin was 5 mm. The axial spatial resolution of the hairpin, i.e. the resolution perpendicular to the face of the hairpin, was determined by fringe electric field effects. For comparison, the spatial resolution of a 3 GHz microwave interferometer is roughly 20 cm.

Diode Laser Absoption for Measuring Metastable State Density

In order to measure the density of $1s_5$ metastable states, we used a New Focus Vortex External cavity diode laser with a maximum output of 18 mW. The wavelength could be varied, using the Vortex power supply, between 811.63 nm (air) and 811.37 nm (air.) The diameter of the beam was 2 mm. The laser was past through the discharge onto a ThorLabs photodiode (10 MHz bandwidth.) The size of the detector was increased, compared to the size of the detector used with the He-Ne laser for deflection signals. Increasing the size of the detector lowered the response rate (bandwidth) of the detector from 100 MHz to 10 MHz. The larger area detector was need so that the deflection of the beam by the neutral density gradient at the shock front would not cause the beam to be deflected off of the detector.

Laser absorption studies have been done by Golubovskii et al. [30] in ionization waves and by Penache et al. [31] in microdischarges. One significant difference with

prior studies is that the laser frequency was purposely set off of the peak resonant frequency of the absorption transition in order to prevent the absorption cross section from changing across the shock front as the gas temperature increases across the shock front. Figure 11 shows absorption of the laser power when the laser frequency was moved off of the absorption peak.
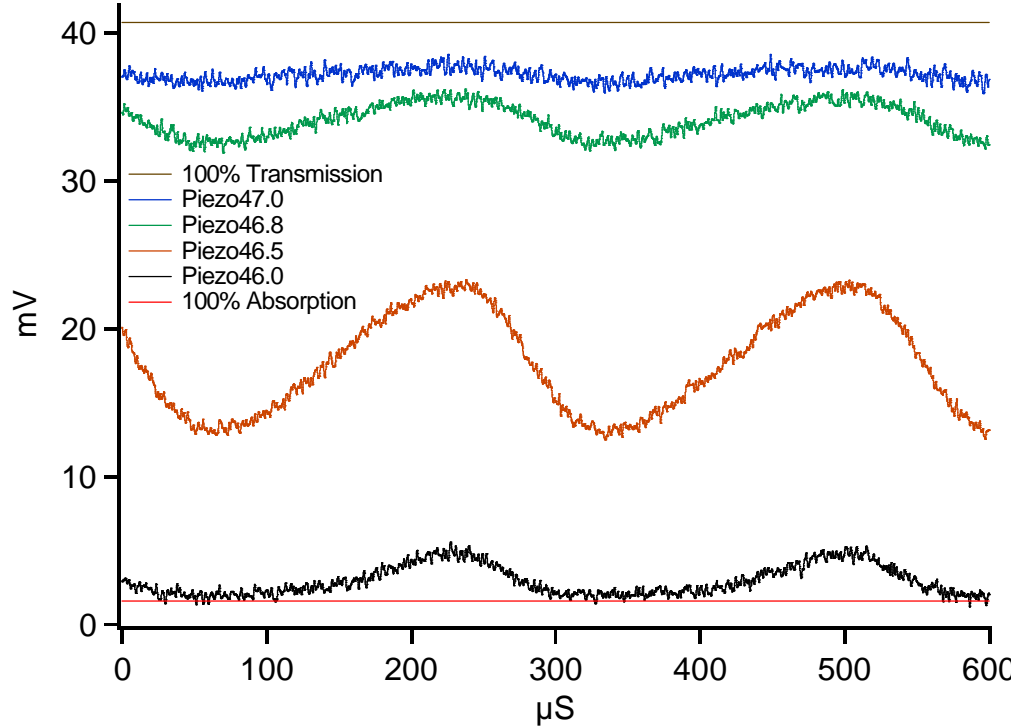
Figure 11: Laser Absorption in Ionization Waves at 0.5 Torr and 14 mA.

In Figure 11, the brown line is the 100% transmission line (i.e. if 100% of the laser power is transmitted through the plasma.) The red line is the 100% absorption line (i.e. if 100% of the laser power is absorbed by the plasma.) This line is not at a value of zero because of stray light from outside the building reaching the photodiode detector. The black line is the detector signal with the laser on the peak resonance of the transition. The orange, green and blues lines are detector signals with the laser wavelength off-peak. As the laser frequency is moved off-peak, less laser power is absorbed by the discharge.

Figure 11 shows that nearly 100% of the laser power is absorbed when the laser sits at the peak of the transition. The equation for laser absorption in a medium, when stimulated emission can be ignored, is Beer's Law.

$$\frac{I}{I_0} = e^{-n_m \sigma(\nu)L}$$

(7)

where I is the laser power after passing through the discharge, I_0 is the laser power before entering the discharge, n_m is the metastable density, $\sigma(\nu)$ is the cross section for the transition, which is a function of the laser frequency, and L is the length of the discharge. Normally, n_m and L are combined into a column density because of the uncertainty of the radial distribution of the metastable density in the discharge. The cross section as a function of frequency is given as

$$\sigma(\nu) = \frac{h\nu}{c} B_{ij} g(\nu), \quad where$$

$$B_{ij} = \frac{A_{ji}c^3}{8\pi h\nu} \quad \& \quad g(\nu) = \frac{c}{\nu_0} \sqrt{\frac{M}{2\pi kT}} \exp\left[-4\ln 2 \frac{(\nu - \nu_0)^2}{(\Delta\nu)^2}\right]$$

(8)

where B_{ij} is the Einstein B coefficient for absorption from level i to level j. A_{ji} is the Einstein A coefficient for spontaneous emission from level j to level i. In our case, the A coefficient from the $1s_5$ to $2p_9$ transition is $3.66 \cdot 10^7$ sec^{-1} [32]. g(ν) is the Gaussian distribution of metastable states due to Doppler velocity broadening.[9] M is the mass of the metastable state. c is the speed of light in a vacuum. ν_0 is the frequency of the peak resonance and $\Delta\nu$ is the half width half maximum of the Gaussian. For argon, $\Delta\nu$ equals $43.95 \cdot T^{\frac{1}{2}}$ in MHz.

---

[9] Collision broadening is negligible below 5 Torr.

The function $g(v)$ is strongly dependent on the frequency of the laser. This dependency is shown in Figure 12 for a range of different gas temperatures. The units of $g(v)$ are GHz^{-1}.
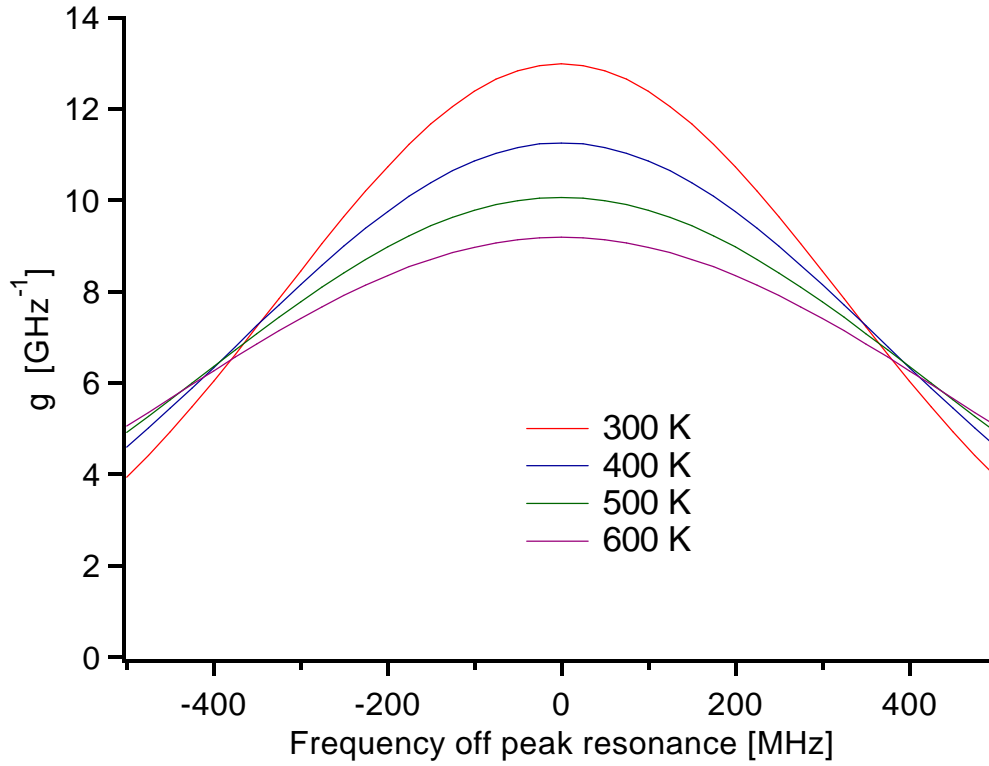
Figure 12: Gaussion Distribution Function g(*v*) versus Laser Frequency Off Peak Resonance

By choosing a value of v such that $v \neq v_0$, the cross section for absorption decreases exponentially squared. This is the reason why the absorption in Figure 11 is less for the orange, green and blue cases than for the black case.

As seen in Figure 12, $g(v)$ is also a function of the temperature of the medium. Therefore, at the shock front there will be a change in $g(v)$ due to the increase in the gas temperature. The temperature behind a shock front is given by Eq (3). For a Mach 2 shockwave, the temperature ratio is 2. Therefore, it was necessary to chose the laser frequency such that $g(v)$ does not change across the shock front. For a Mach 2 shockwave, $g(300\ K) = g(600\ K)$ when $(v - v_0) = \frac{1}{2} \Delta v(300\ K)$. For experiments with a

Mach 2 shockwave, the laser frequency was kept at the half-width of the 300 K Gaussian (380 MHz off-peak) in order that there would be no change in $g(v)$, and hence no change in the cross section, σ, as the shockwave passed through the laser beam. For each Mach number used, $g(T_1) = g(T_2)$ was solved in order to determine how far off of resonance to set the laser frequency. As seen in Figure 12, the 400 K and 500 K curves cross the 300 K curves as frequencies only slightly to the left of where the 600 K curve crosses the 300 K. Therefore, if there were an uncertainty in the Mach number or laser frequency, this would introduce only a small error in the metastable state density.

Diode laser absoption spectroscopy (DLAS) was employed to measure the density of $1s_5$ metastable states. There are two dominate metastable states in argon. In LS notation the states are labeled as $^3P_2$ and $^3P_0$. In Paschen notation, the states are labeled $1s_5$ and $1s_3$, respectively. There are two nearby resonance states labeled $1s_4$ and $1s_2$. These states are a mixture of $^3P_1$ and $^1P_1$ states. LS notation does not hold for the resonance states because L and S are not good eigenvalues. Only J is a good eigenvalue. So, the two J=1 states mix. Only Paschen notation will be used in the thesis for the metastable states and the excited states; the LS coupling notation is just for informational purposes. The ground state ion, $^2P_{3/2}$, is 15.8 eV above the ground state neutral, $^1S_0$. The $1s_3$ metastable is 11.72 eV above the ground state and the $1s_5$ metastable is 11.55 eV above the ground state. The radiative lifetime of the $1s_3$ metastable state is 45 seconds [32]. The radiative lifetime of the $1s_5$ metastable state is 55 seconds [32]. For these states, electric dipole transitions to the ground state are forbidden. Figure 13 (next page) summaries the energy levels in argon. The four 1s states are shown on the left side of this figure and the 2p states just to the right and a few eV above the 1s states. There are a total of ten 2p excited states. The emission studied in this thesis is from the $2p_6$ state to the $1s_5$ state (red arrow). The absorption (light blue arrow) is from the $1s_5$ to the $2p_9$ state. The LS notation for the $2p_9$ state is $^3D_3$ and the LS notation for the $2p_6$ state is $0.2280\,^3D_2 + 0.5866\,^1D_2 + 0.7710\,^3P_2$, meaning that there is mixing of LS states with similar total angular momentum [33]. The number of the state and its value of total angular momentum, j, are shown at the top of the figure.

Figure 13: Energy Level Diagram of Argon

The metastable states are quenched by inelastic collisions with air impurities, superelastic collisions with electrons, and collisions with electrons causing the metastable state to become a nearby resonance states. The $1s_4$ resonant state can radiate to the $^1S_0$ ground state in 8.4 nanoseconds and the $1s_2$ resonant state can radiate to the $^1S_0$ ground state in 2.0 nanoseconds. Figure 45 in Appendix A suggests that the principal loss mechanism of metastable states is collisions with air impurities. The rate constant for the quenching of $1s_5$ by N_2 is 3.4×10^{-11} cm^3/sec [34]. This inelastic collision quenches the argon metastable into the ground state and excites the ground nitrogen molecule into the C $^3\Pi_u$ state. Using the rate constant above and assuming a nitrogen impurity level of 10 mTorr (or 1% for 1 Torr Argon), the quenching rate is 1×10^4 1/sec or a mean life time of 100 μs. The quenching of argon metastables by nitrogen impurities will be used in the Analysis Section of the thesis to explain some of the results collected with shockwaves.

III.   Results

The results section is broken down into the following main sections: electron compression at the shock front in steady-state discharges; double layer potential at the shock front in steady-state discharges; characterization of discharges with ionization waves; and finally, shockwaves into discharges with ionization waves.

Electron Compression at the Shock Front

The electrons have a thermal velocity two orders of magnitude larger than the shock velocity, but they can be compressed at the shock front because their density must closely follow the positive ion density. Figure 14 shows the electron number density before, at and after the shock front for two different Mach numbers. The data is collected using the time-dependent hairpin resonator technique mentioned briefly in the experimental set up section.
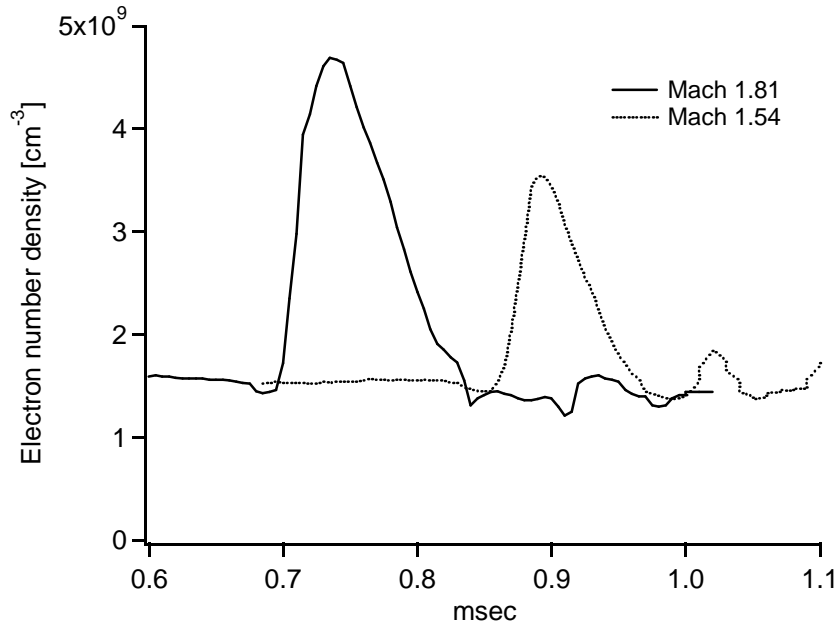

Figure 14: Electron Number Density at Two Shock Fronts

26

In Figure 14, the discharge pressure was 0.5 Torr and the shockwave traveled from the anode to the cathode. Only the Mach number of the shockwave varied. The discharge current was kept below the threshold for ionization wave formation. Figure 14 shows an increase of electron number density at the shock front. Behind the shock front, the electron number density slowly decays. Data was also collected in the argon afterglow where the electron temperature is significantly lower than in a steady state discharge, so that electron impact ionization could not occur at the shock front and so that there is no applied electric field to affect the fluxes of electrons at the shock front double layer.
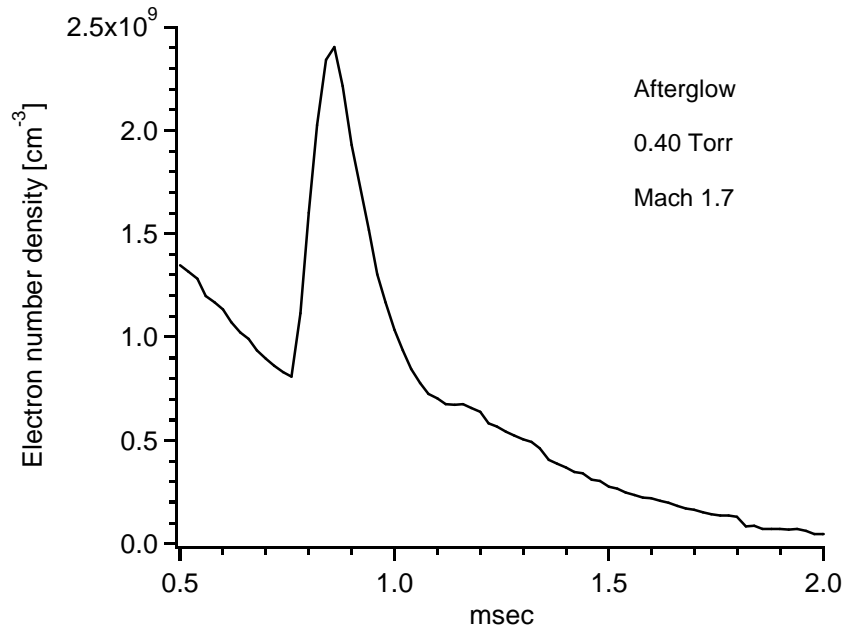
Figure 15: Electron Density at Shock Front in Afterglow

The electron number density rises very slowly at the shock front in Figure 15. In the afterglow, the rise in electron number density should be rapid because the electron Debye length is quite small compared to the steady state cases in Figure 14. The cause of the slow 100 μsec rise time is not known. The spatial resolution of the hairpin can not be the cause of the slow rise time because the neutral particle shockwave passes through the 5 mm of the hairpin resonator in 10 μsec. The ratio of the electron number density after the shock front to before the shock front is graphed in Figure 16 for the two cases in

Figure 14 and for two afterglow cases. Also plotted in the figure are the density ratios for the neutral species given by the Rankine-Hougoniot relationship and for electrons numerically solved by Adamovich et al. [2].
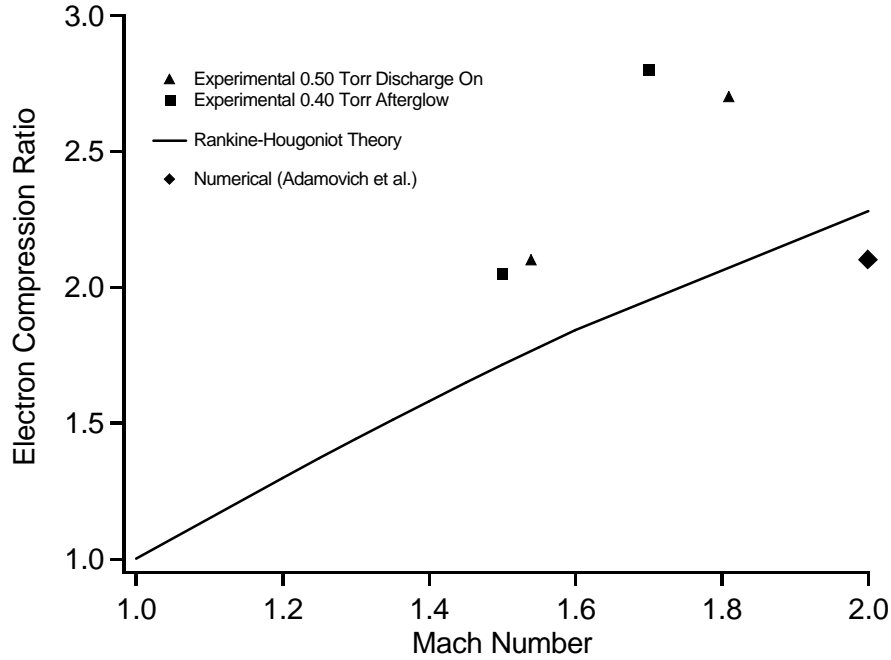
Figure 16: Comparison of Density Ratio at Shock Fronts

For the four cases studied, the ratio of electron number density after the shock front to the electron number density before the shock front is larger experimentally than would be predicted for the ratio of the ground state neutral number density. On the other hand, the numerical simulation by Adamovich et al. [2] at 10 Torr argon predicted an electron density ratio slightly less than the Rankine-Hougoniot relationship.

In order to determine the location of the light emission enhancement with respect to the electron number density enhancement, a fiber optic detector was placed collocated with the hairpin resonator. Figure 17 shows the electron number density and 763 nm light emission when a Mach 1.55 shockwave travels into a stable 2.86 mA 0.64 Torr discharge.

Figure 17: Electron Number Density and Light Emission at Mach 1.55 Shock Front

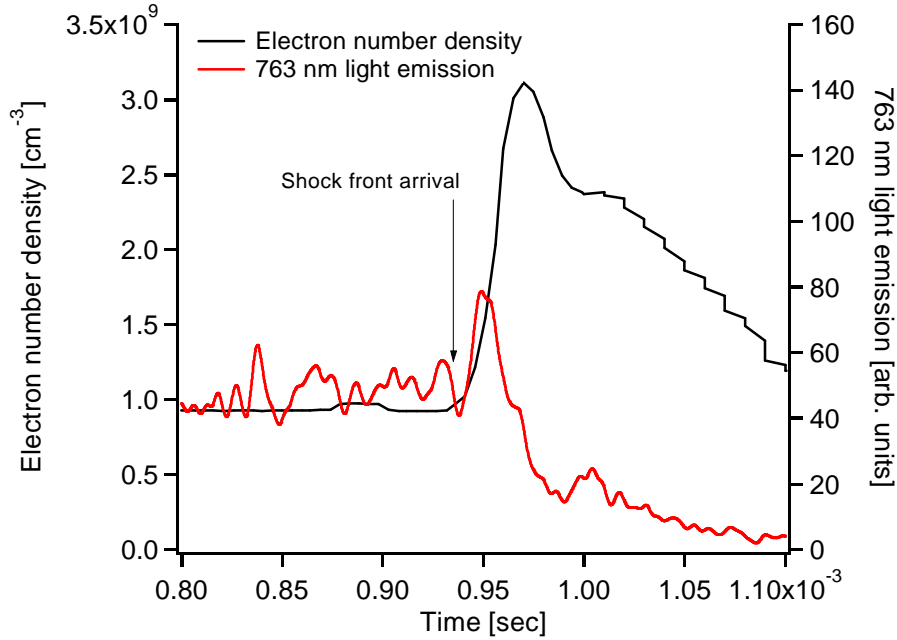There is a small jump in the light emission and a rather noticeable jump in the electron number density at the shock front. The peak electron number density lags behind the behind the neutral density shock front and the peak in light emission by roughly 30 μsec. The reason for this delay can not be due to the hairpin resonator because the hairpin resonator can respond to a changing electron number density in less than 1 μsec. The peak electron number density in the afterglow lagged behind the shock front by 120 μsec. In Figure 15, the shock front arrived at t=760 μsec, but the peak in electron number occurred at t=880 μsec. The reason for this discrepancy is not known.

Double Layer Potential: Experiment vs. Theory

In this section, the potential of the double layer was measured as a function of Mach number using two floating probes and compared with theory. The following two figures show floating probe voltage difference signals. In all cases, the shockwave traveled from the cathode to the anode in the active discharge. The pressure for the data

in Figure 18 was 2 Torr and the pressure for the data in Figure 19 was 1 Torr. The discharge current in both cases was 1.3 mA. The discharge current was kept below the threshold for ionization wave formation so that the shockwave arrives into a steady-state discharge. The discharge electric field before the shock front arrived in the first case was 8 Volts / 2 cm or 4 V/cm. The *E/p* was 2 V/(cm×Torr).

After the initial steady-state voltage difference, there was a drop and rise in floating probe voltage difference. The rapid drop occurred as the double layer crossed the plane of the first floating probe and the rapid rise occurred after the double layer traveled past the second floating probe. The drop was not instantaneously either because of the RC time of the floating probe or because of the lag in the peak electron number density seen in previous figures. The width of the rise-and-fall decreased with increasing Mach number because the transit time through the 2 cm separating the floating probes decreased.
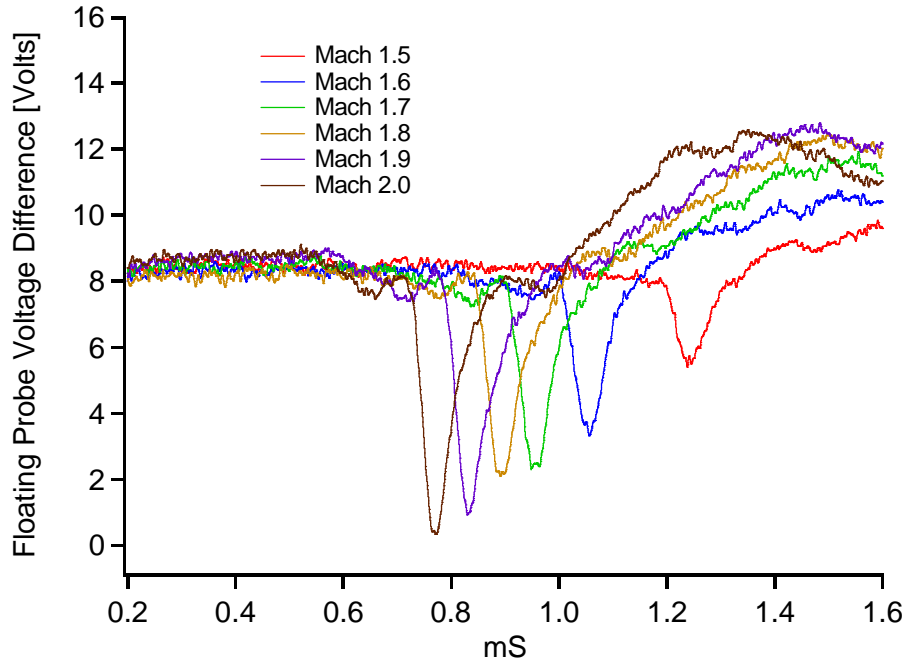

Figure 18: Floating Probe Potential at Mach 2 Shockwaves in 2 Torr 1.3 mA Discharge
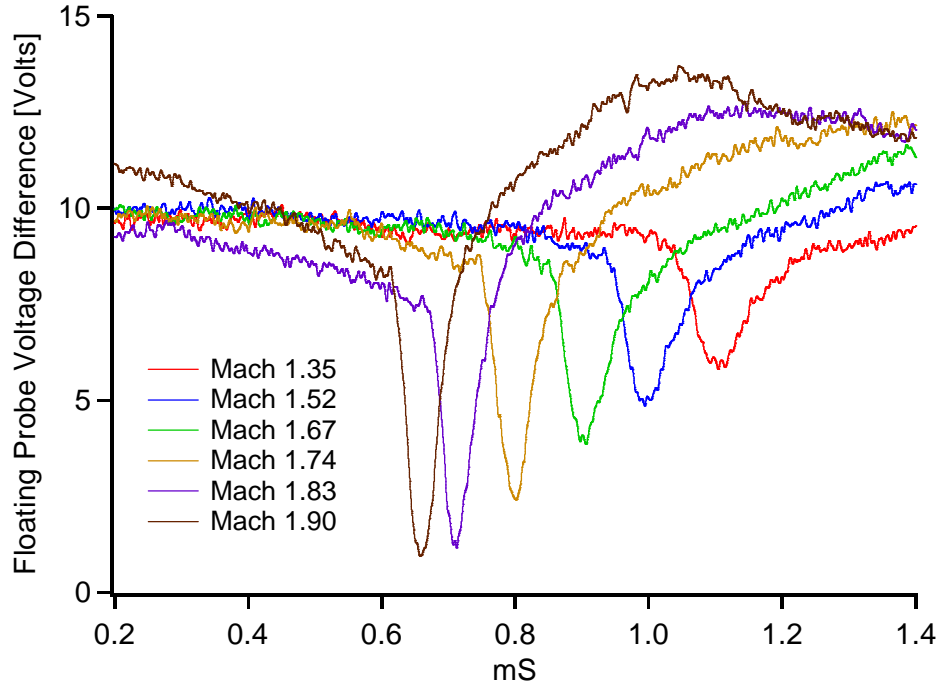
Figure 19: Floating Probe Potential at Mach 2 Shockwaves in 1 Torr 1.3 mA Discharge

The double layer potential increased with Mach number in both the 1 Torr and 2 Torr cases. After the double layer passed by both probes, the discharge tried to reestablish a steady-state mode. In these figures, the double layer appears negative, but this was due to the fact that the probe downstream was subtracted from the one upstream. The actual double layer potential was positive, meaning that the potential increased across the shock front. The potential difference at the shock front is graphed in Figure 20 from the experimental results in Figure 18 and Figure 19. Also included in Figure 20 is the theoretical double layer potential calculated by Jaffrin [1] for the case of $T_e = T_i$ before the shock front and the double layer numerically calculated by Adamovich et al. [2] where $T_e = 3.6$ eV. In this figure, the double layer potential is normalized by the electron temperature behind the shock front so that a comparison can be made between theory and experiment.

Figure 20: Normalized Double layer Potential at Shock Fronts

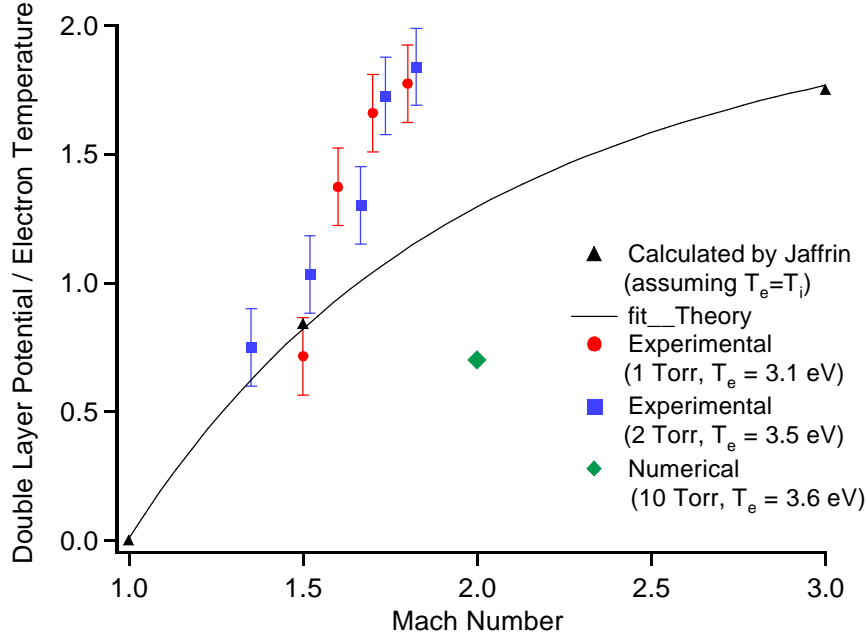The calculated double layer potential is Jaffrin's Eq (5.28): $\Phi/kT_e = ln(\rho_2/\rho_1) + \Phi_3$, where $ln(\rho_2/\rho_1)$ is a term similar to the Boltsmann distribution $n_{e2}/n_{e1} = e^{-\Phi/kTe}$ and where Φ_3 is a term mentioned, but not explicitly derived in the Jaffrin text. The experimental double layer potentials were divided by the electron temperature at the shock front, using the *E/N* value before the shockwave arrives as an input into the numerical code BOLSIG [35]. The numerically estimated mean electron energy was 4.7 eV at 2 Torr and 5.3 eV at 1 Torr, which corresponds to an electron temperature of 3.1 eV and 3.5 eV, respectively.[10] The experimental double layer potential (red and blue) and the theoretical potential (black) roughly match with each other at lower Mach number, but for larger values of Mach number. The one data point by Adamovich et al. [2] is below both the experimental results and the analytic results. Jaffrin [1] only calculated the double layer potential for

---

[10] The electron energy distribution function in argon is not Maxwellian. The temperature was calculated by taking the mean energy and multiplying by two thirds. The difference between the theory and experiments may be due to the fact that a different electron temperature should be used.

three cases: Mach 1.5, Mach 3 and Mach 10 (not shown.) A curve was fit through these data points. In the theory by Jaffrin [1] the electron temperature equaled the gas temperature, the electron Debye length was much less than the shock thickness and the electron drift velocity was zero; however, it seems possible to use the Jaffrin theory to determine the approximate double layer potential at the shock front in non-equilibrium plasma by substituting the equilibrium electron temperature behind the shock front with the non-equilibrium electron temperature before the shock front. The reason for the discrepancy between the experimental and theoretical results could be the fact that there is an applied electric field in the direction of the shock wave propagation.

Ionization Waves Only

For the rest of the data collected, the discharge current was increased so that ionization wave appeared. This allowed the light emission, electric field, electron number density and metastable state density to fluctuate versus time. A few graphs of these fluctuations without shockwaves are presented before adding shockwaves. Figure 21 shows the 763 nm light emission and the electric field versus time for ionization waves when the gas pressure was 1 Torr and the discharge current was 10 mA.
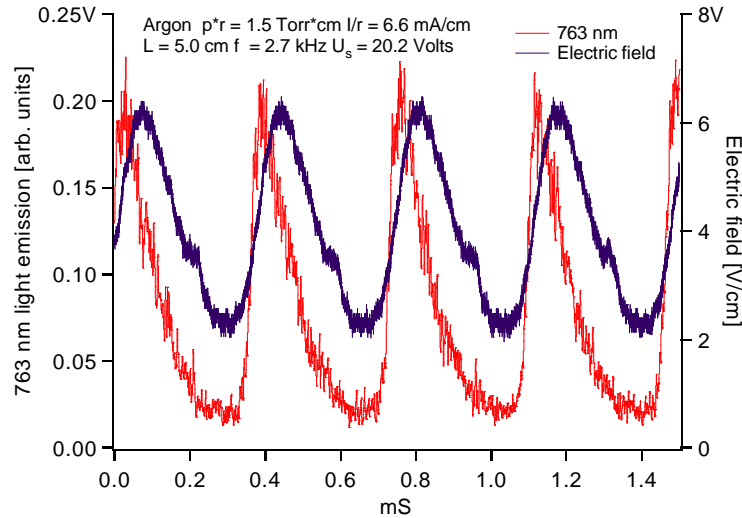

Figure 21: 763 nm Light emission and Electric field in 1 Torr, 10 mA Ionization Wave

33

In Figure 21, there is a roughly +/-100% fluctuation in the light emission, but only +/-50% for the electric field. The wave frequency is 2.7 kHz. There is a thirty degree phase difference between the light emission and the electric field in this case. The current, not shown, was constant. The current is given by

$$j_x = -e\mu_e En_e - eD_e\,\partial n_e\big/\partial x = const. \qquad\qquad , \qquad\qquad (9)$$

where j_x is the current density, e is the elementary charge constant, μ_e is electron mobility, E is the electric field, n_e is the electron number density, D_e is the electron free diffusion coefficient, and $\partial/\partial x$ is the gradient along the axial direction.

Figure 22 shows the electron number density and the $1s_5$ metastable state density for an ionization wave at 0.5 Torr and 16 mA. The electron number density was collected using the boxcar approach with the hairpin resonator. There is a phase difference of 60 degrees between the peak in the metastable state density and peak in the electron number density.
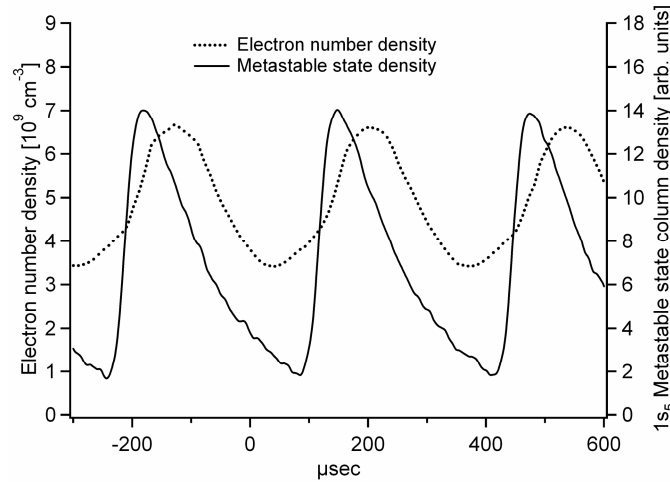

Figure 22: Electron and Metastable Density in Ionization Wave

The wave frequency in Figure 22 was 3.06 kHz. One difficulty in collecting the electron number density show in Figure 22 is that the wave frequency had a tendency to change over time. The boxcar approach takes roughly one hour to collect the data.

Figure 23 shows the 763 nm light emission and the $1s_5$ metastable column density at 2 Torr and 30 mA. The wave frequency was 3.5 kHz.
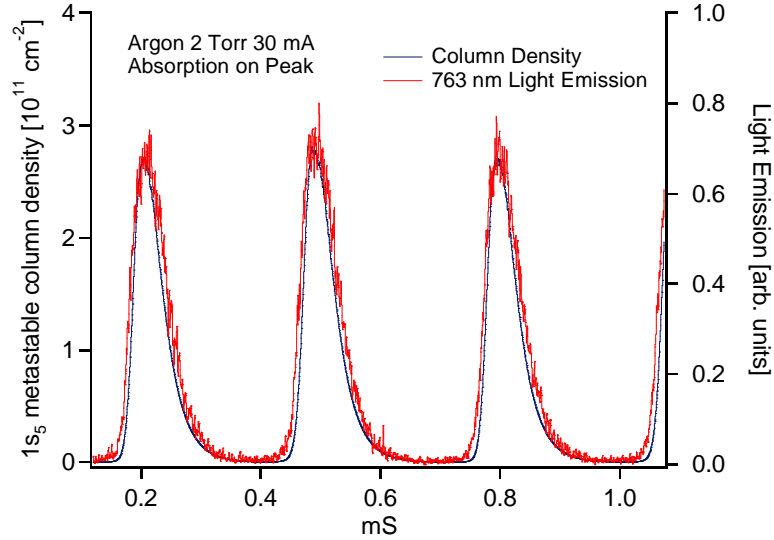
Figure 23: 763 nm Light emission and $1s_5$ Metastable Column Density at 2 Torr 30 mA

The metastable density is given in units of cm^{-2} as a column density, $\int n_m \, dL$.[11] In Figure 23, the $1s_5$ metastable density fluctuates +/- 100%, just as the light emission does at this pressure and current.

Shockwaves in Ionization Waves: Light Emission and Electric Field

The next step was to send shockwaves into discharges with ionization waves. In Figure 24 to Figure 32, the shockwave traveled in the direction from the anode to the cathode. Figure 24 shows the light emission and floating probe difference when a Mach 2 shockwave travels into a 1 Torr 30 mA discharge. For these figures, the fiber for light

---

[11] In the rest of the figures, it was necessary to sit off the peak resonance and, therefore, the metastable density is not given in absolute units. In the rest of the figures, the term metastable density and metastable column density are used interchangeable because the units are relative rather than absolute.

emission was placed half way between the two floating probes. In Figure 24, the detectors saw a full ionization wave and then part of another wave before the shockwave arrived. Also shown in the figure is one ionization wave after the shockwave passed by the detectors.
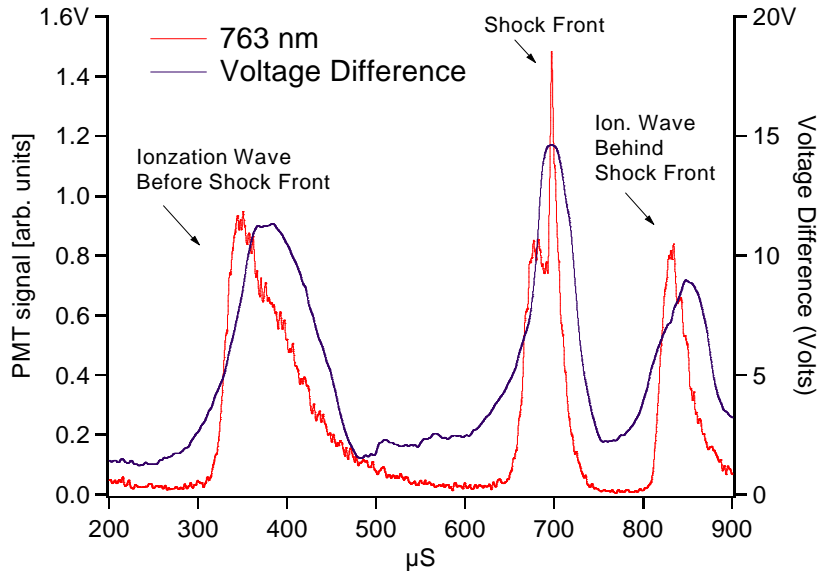
Figure 24: Light Emission and Floating Probe Difference when Mach 2 Shockwave Arrives near Peak

Figure 24 shows the light emission and voltage difference when a Mach 2 shockwave arrives near the peak of the ionization wave. There is a sharp rise in the light emission and a slow rise in the voltage difference. The voltage difference rise at the shock front is slower than the emission rise because of the 2 cm spatial resolution of the two floating probes, compared with the 1 mm spatial resolution of the optical fiber. For both variables, the maximum value at the shock front was greater than the value at the peak of earlier ionization waves. After the initial rise, there was a rapid drop in the voltage difference and in the light emission. An ionization waves appeared 100 μs after the shock front.

In Figure 25, the same Mach 2 shockwave was sent into the discharge; however, in this figure, the shockwave arrives at a different phase of the ionization wave.
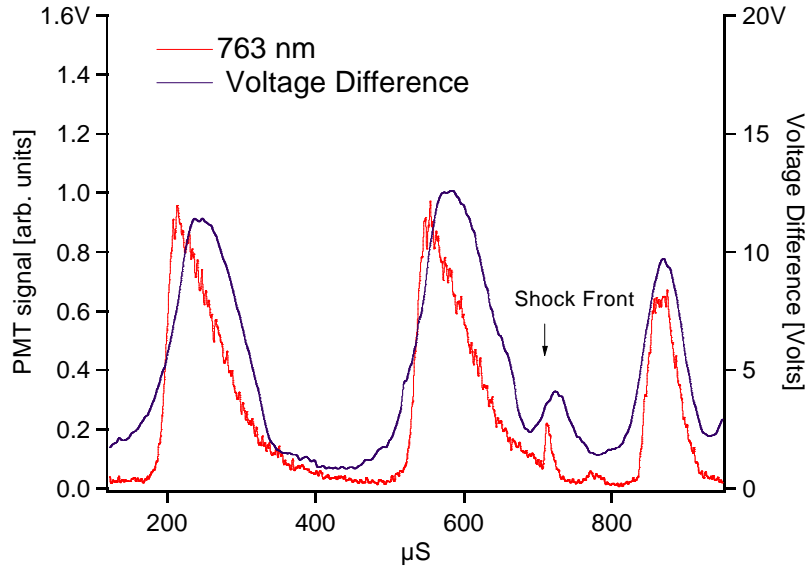
Figure 25: Light Emission and Floating Probe Difference when Mach 2 Shockwave Arrives near Valley

This time, the light emission enhancement at the shock front is significantly smaller than in the previous figure. The electric field enhancement is smaller than in Figure 24, but only slightly. Once again, an ionization wave follows behind the shock front. The polarity of the voltage jump is positive in both Figure 24 and Figure 25. In Figure 24, the voltage jump is approximately +3 Volts, and in Figure 25, the voltage jump is approximately +2 Volts. Qualitatively, it makes sense that the voltage jump is greater when the shockwave arrives at the peak compared with the valley because the electron temperature is greater at the peak than in the valley. As was shown in Figure 20, if the Mach number is kept constant, then the double layer potential should be linearly proportional to the electron temperature. The voltage jump appears positive and is positive when the shockwave is sent anode to cathode, as opposed to it appearing negative in Figure 18 and Figure 19 when the shockwave is sent cathode to anode. The reason for this is now presented.

When the shockwave travels from the anode to the cathode, the floating probe difference is A minus B, where A is the floating potential on the probe nearest anode and B is the floating potential on the probe nearest the cathode. When the shockwave travels from the cathode to the anode, the floating probe difference is once again A minus B. However, the probes A and B have been swapped so that the floating potential difference

in the steady-state discharge appears positive. When the shockwave travels from the anode to the cathode, it passes by probe A and then it travels 2 cm downstream, passing by probe B. When the shockwave travels from the cathode to the anode, it passes by probe B first and then it travels 2 cm downstream, passing by probe A. This is the reason why the double layer at the shock front appears to be positive in Figure 24 & Figure 25 and appears to be negative polarity in Figure 18 & Figure 19. In fact, the double layer is always positive with respect to the direction of the shock front, as expected from theory.

The following figure shows an interesting feature of sending shockwaves into argon glow discharges. The discharge current remains constant.
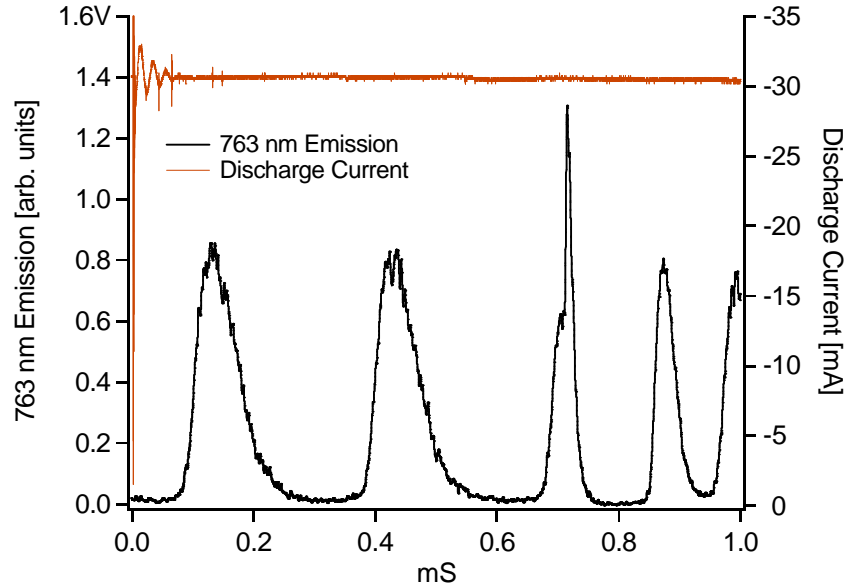
Figure 26: Light emission and Discharge Current at 2 Torr, 30 mA, Mach 2

In Figure 26, the shockwave arrived near the peak of the ionization wave and traveled from the anode to the cathode. The global discharge current does not vary, even though there are ionization waves and a shockwave in the discharge. The fluctuations near t=0 were electrical noise from the creation of the shockwave, which does not affect the fiber optic signal. This figure also shows that the frequency of the ionization waves after the shock front was nearly twice the frequency of the ionization waves before the shock front

arrived. More graphs from this data run (2 Torr, 30 mA, Mach 2) are included in Appendix B.

The next step was to analyze the light emission enhancement for shockwaves arriving at a variety of different phases of the ionization wave. For the data set that makes up Figure 27 and Figure 28, the Mach number, the flow rate, the pressure and the current were kept constant. In Figure 27, the light emission enhancement is plotted versus phase of the ionization wave. [12] The enhancement is defined as the peak light emission at the shock front minus the light emission right before the shock arrival.
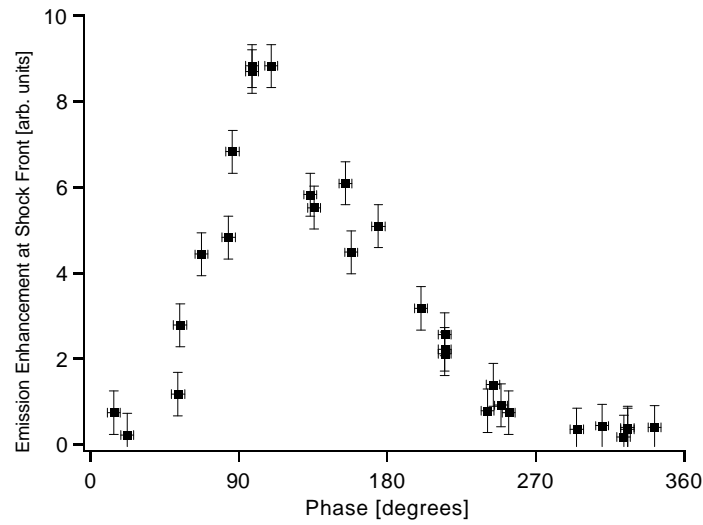
Figure 27: Light Emission Enhancement versus Phase

In Figure 28, the ratio of the peak light emission to the light emission before the shock arrival is plotted using the same data from Figure 27.

[12] Zero degrees is arbitrarily defined as the location of the minimum light emission. 115 degrees is the location of the maximum light emission. The location of the maximum light emission is not 180 degrees because the ionization waves are not sinusoidal, i.e. the waves are nonlinear rather than linear.
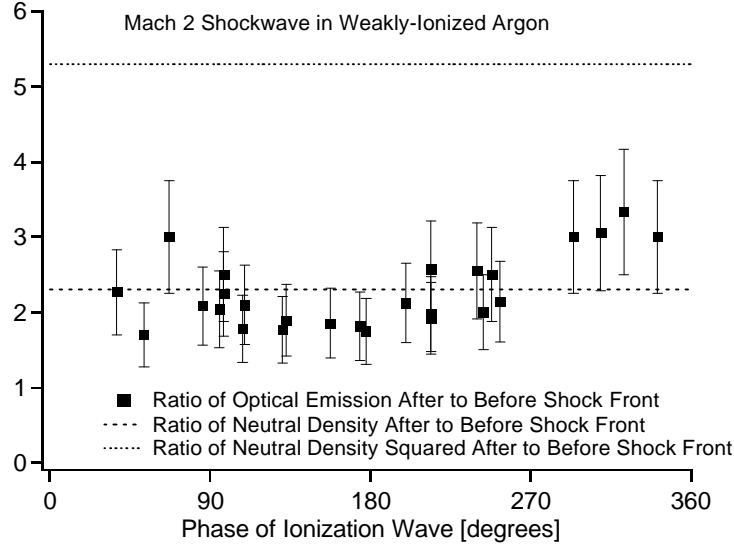
Figure 28: Ratio of Light Emission after to before Shock Front versus Phase

Note that in Figure 27 the enhancement in light emission at the shock front, as a function of phase, is the same shape as the ionization wave itself. This suggests that the light emission enhancement at the shock front is due to compression of particles at the shock front. This conclusion is further supported in Figure 28 because the ratios of light emission across the shock front fall roughly around a straight line.

If excited $2p_6$ states could be compressed at the shock front, then this could explain the light emission enhancement. However, excited $2p_6$ states can not be compressed at the shock front because their radiative lifetime (36 ns) is less than the time to travel through the shock front (~200 ns). This means that the density of excited $2p_6$ states is always a function of the electron number density, the electron energy distribution function (EEDF) and the metastable state density.[13]

Figure 28 shows the ratio of 763 nm emission after the shock front to that before the shock front. The two straight lines show the values 2.3 and 5.3, which are the values

---

[13] This assumes that the production of $2p_6$ states is due to electron step-wise excitation from the $1s_5$ metastable state.

(ρ_2/ρ_1) and $(\rho_2/\rho_1)^2$ for a Mach 2 shockwave in an atomic gas, as given in Eq (2). The analysis chapter of this thesis will show that, if the electron number density remained constant, the EEDF remained constant and the metastable density increased across the shock front by (ρ_2/ρ_1), then the light emission would increase by a factor of (ρ_2/ρ_1). If, however, the electron number density increased across the shock front by (ρ_2/ρ_1), the EEDF remained constant and the metastable density increased across the shock front by (ρ_2/ρ_1), then the light emission would increase by a factor of $(\rho_2/\rho_1)^2$. Therefore, the straight lines in Figure 28 show the expected increase in light emission if a) only the metastable states are compressed and b) the metastable states and electrons were compressed.

Shockwaves in Ionization Waves: Metastable State Density

In theory, metastable states can be compressed at a shock front because their lifetime (~100 μsec) is greater than the time needed to transit through the shock front. To prove this, we measured the density of $1s_5$ states when a shockwave is sent into the afterglow. In the afterglow, there is no way to produce new metastable states, so if there is an increase in density, it must be due to compression at the shock front. Figure 29 shows the light emission and $1s_5$ density before and after the discharge is switched off.
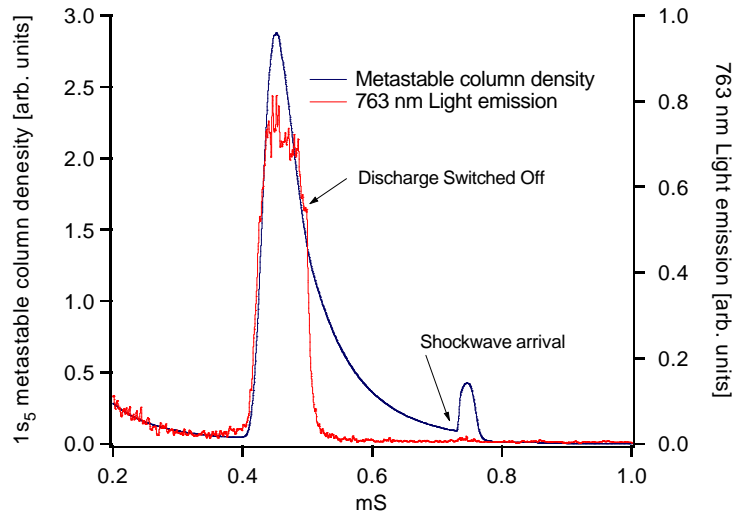

Figure 29: 763 nm light emission and $1s_5$ metastable state density for Mach 2 shockwave in the afterglow

41

In Figure 29, after the discharge was switched off, the light emission rapidly dropped to zero, whereas the metastable density slowly decayed. At the shock front, there was an increase in the metastable state density. This increase suggests that metastable states can be compressed at a shock front. The measured ratio of metastable state densities in Figure 29 is 2.9 ± 0.5 and the predicted value for the density ratio from Eq (2) is 2.3. This process was repeated at five other Mach numbers. Figure 30 shows the experimental and predicted value for the density ratio as a function of Mach number.
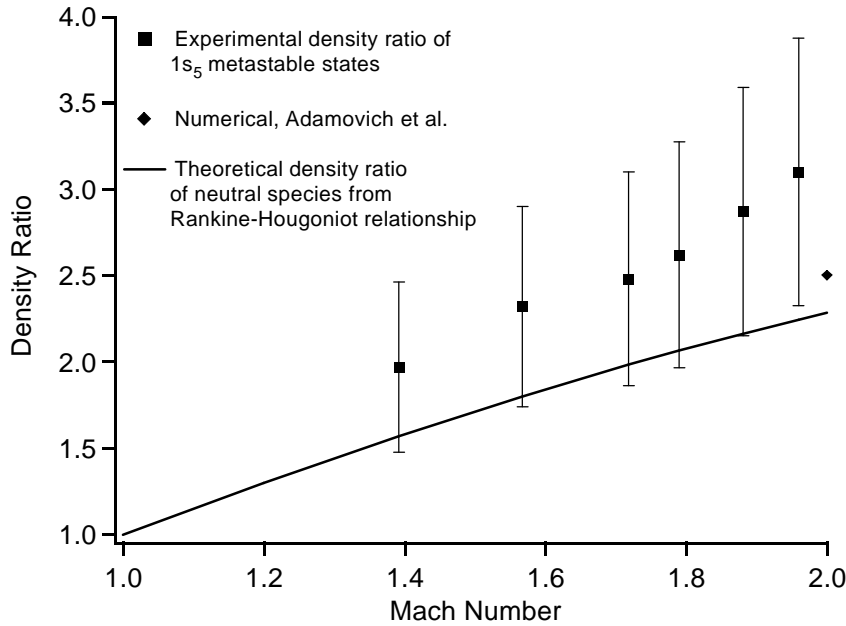
Figure 30: $1s_5$ Metastable State Density Ratio versus Mach number

In Figure 30, the density ratio was always larger than the value expected by the Rankine-Hougoniot relationship. The large error bars are due to the fact that the absorption cross section depends sensitively on the frequency of the laser and that a wave-meter was not used to measure the exact laser frequency. As stated earlier, this set of data was collected in the argon afterglow. The electron temperature in the afterglow is nearly room temperature. This is why the light emission rapidly decreases when the

discharge voltage is switched off in Figure 29. With only cold electrons in the afterglow, there is no way for new metastable states to be created at the shock front, which means that the Rankine-Hougoniot relationship should be valid here. Yet, the one data point calculated by Adamovich et al. [2] suggests that the overshoot may actually be real.

Metastable states can be locally compressed at the shock front because their effective lifetime is greater than ~200 ns it takes particles to travel through the shock front. When the ground state argon atoms are being compressed at the shock front, the metastable states are also being compressed because they can't get out of the volume being compressed. They can, however, be collisionally quenched by impurity molecules or converted into resonance states ($1s_2$ or $1s_4$). So, their density far from the shock front will once again be a function of the discharge reduced electric field, *E/N*, (production) and the impurity density (losses.) Figure 31 & Figure 32 show that, in the active discharge, the light emission and metastable state density match each other just as in the ionization wave.
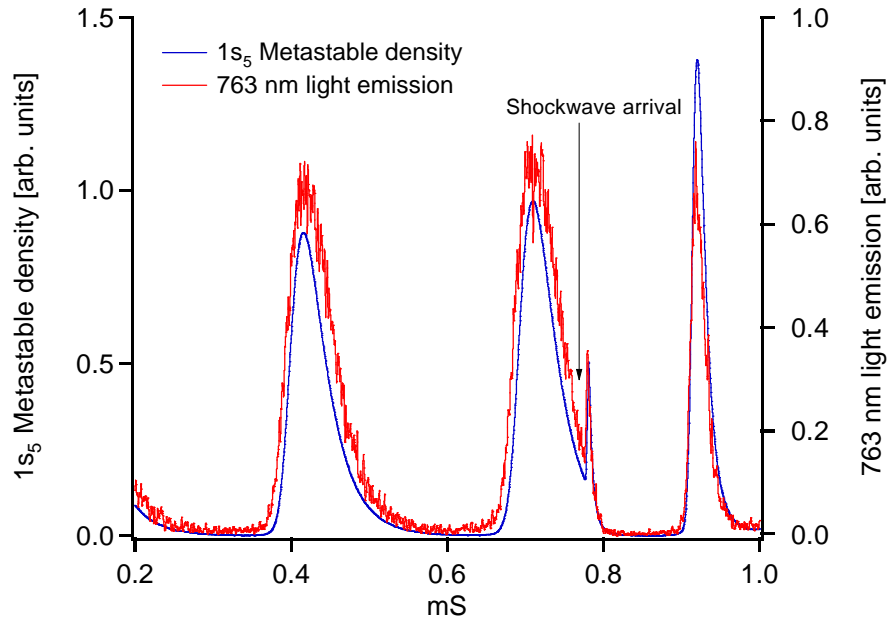
Figure 31: Light Emission and Metastable Density in 2 Torr 30 mA Discharge when a Mach 2 Shockwave Arrives near the Valley
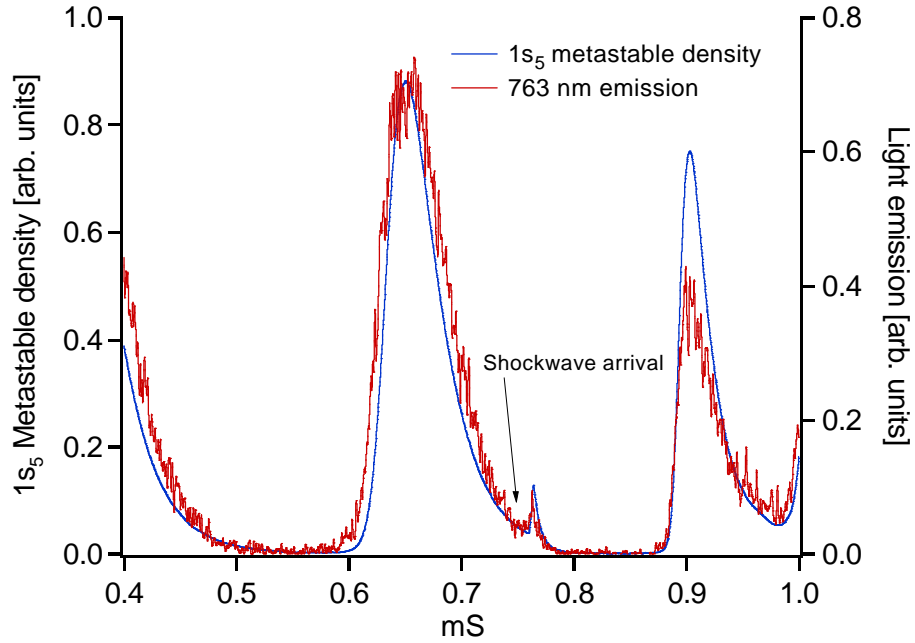
Figure 32: Light Emission and Metastable Density in 2 Torr 30 mA Discharge when a Mach 2 Shockwave Arrives at the Valley

The light emission and the metastable state density in Figure 31 and Figure 32 both increase with the same ratio at the shock front. This, along with the results in Figure 28, suggests that the light emission enhancement at the shock front can be explained solely by the compression of metastable states at the shock front. This analysis is continued in section IV. As expected, the ratio of metastable state density across the shock front in the afterglow (Figure 29) was the same as the ratio of density across the shock front in the active discharge (Figure 31 and Figure 32). This means that new metastable states were not made at the shock front, but rather their density increased due to compression.

Shockwaves in Ionization Waves: Polarization Dependence

The goal of this subsection is to show the dependence of the light emission enhancement, metastable density and double layer potential on a reversal of the polarity

of the discharge with respect to the shockwave direction, i.e. switching the location of the cathode and the anode. Figure 33 and Figure 34 show the light emission and metastable state density when the shockwave traveled from the cathode to the anode. Note that in Figure 31 and Figure 32 the shockwave traveled from the anode to the cathode.
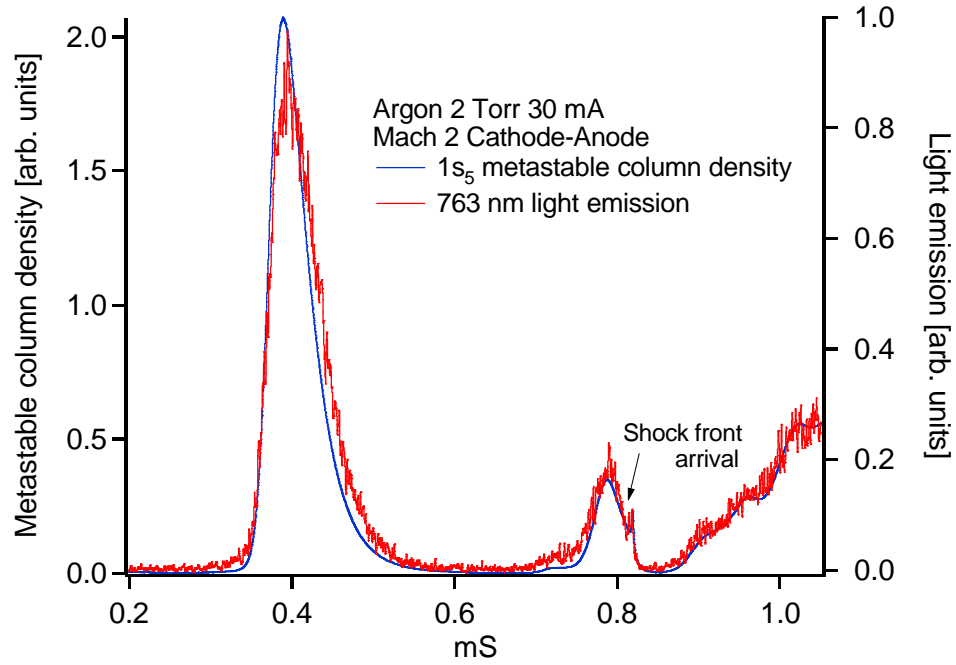
Figure 33: Light Emission and $1s_5$ Metastable State Density when a Mach 2 Shockwave Arrives on Back Side of Ionization Wave

There are some clear differences between the cathode to anode data in Figure 32 and the anode to cathode data in Figure 33. First, the ionization wave (upon which the shockwave arrives) is distorted in Figure 33 compared to the ionization wave well before the shock front. Second, the ionization wave behind the shock front is not really an ionization wave, but a slow steady increase in light emission and metastable column density.
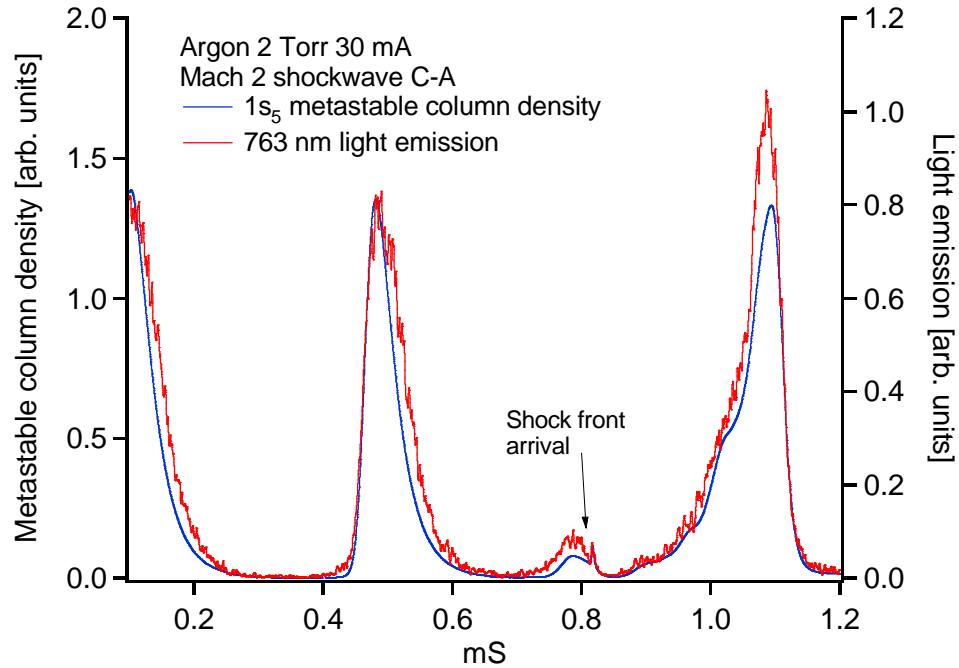
Figure 34: Light Emission and $1s_5$ Metastable State Density when a Mach 2 Shockwave Arrives at what Should be the Front Side of the Ionization Wave

Once again, Figure 34 shows that the shockwave altered the structure of ionization wave when the shockwave traveled cathode to anode. The timing of the shockwave was such that it should have arrived at the front side of the ionization wave. However, the shockwave distorted the ionization wave (essentially turning it off before its normal peak.)

Figure 35 through Figure 38 (next pages) show the 763 nm light emission and floating probe difference signals for Mach 2 shockwaves in 2 Torr 30 mA discharges. In the first two figures, the shockwave traveled from the anode to the cathode. In the second two figures, the shockwave traveled from the cathode to the anode. The difference between A minus B probe subtraction and B minus A probe subtraction is why the double layer appears positive in the first two figures and appears negative in the second two figures.

Figure 35: Light Emission and Floating Probe Difference: Anode-Cathode at Valley
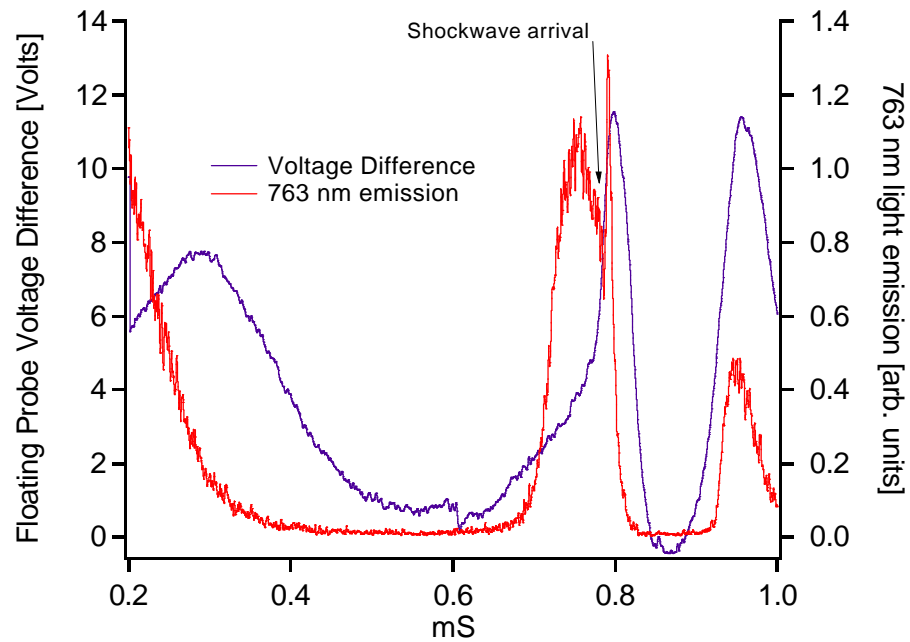
Figure 36: Light Emission and Floating Probe Difference: Anode-Cathode near Peak

47
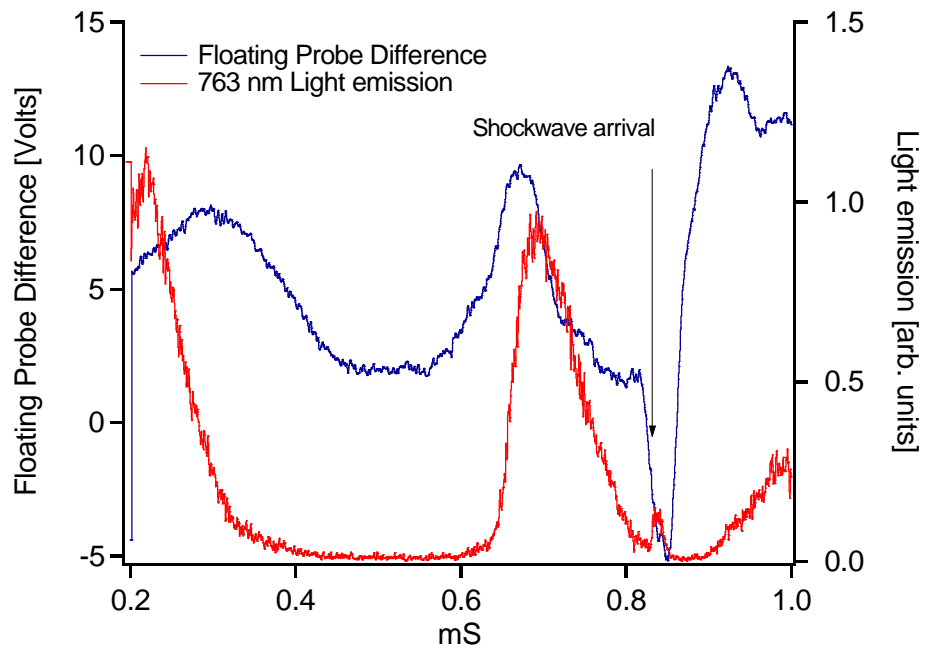
Figure 37: Light Emission and Floating Probe Difference: Cathode-Anode at Valley
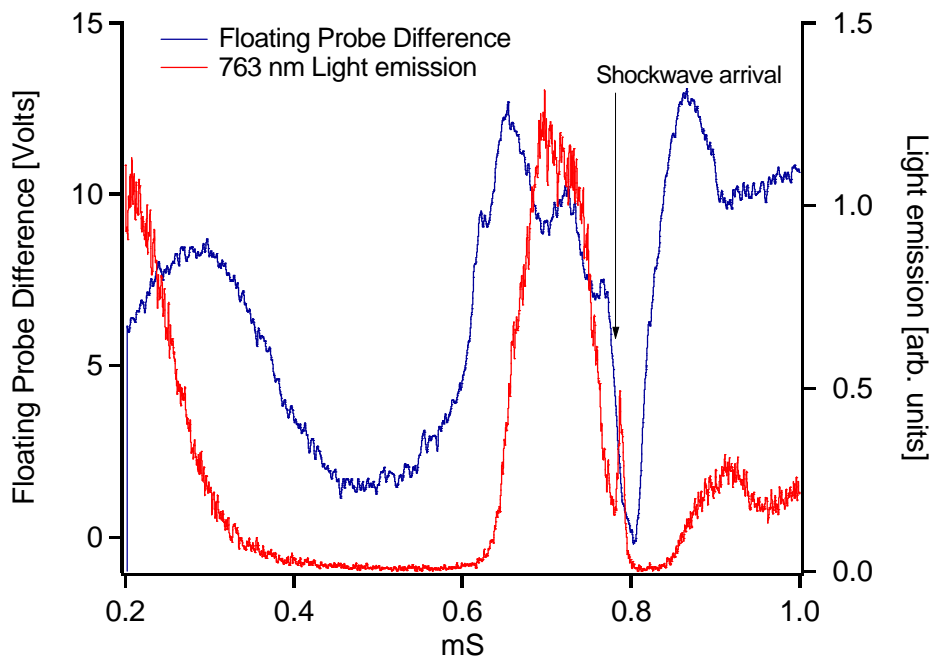
Figure 38: Light Emission and Floating Probe Difference: Cathode-Anode near Valley

In Figure 35, the shockwave arrived when the electron temperature was at its minimum in the ionization wave (~3.5 eV).[14] The enhanceme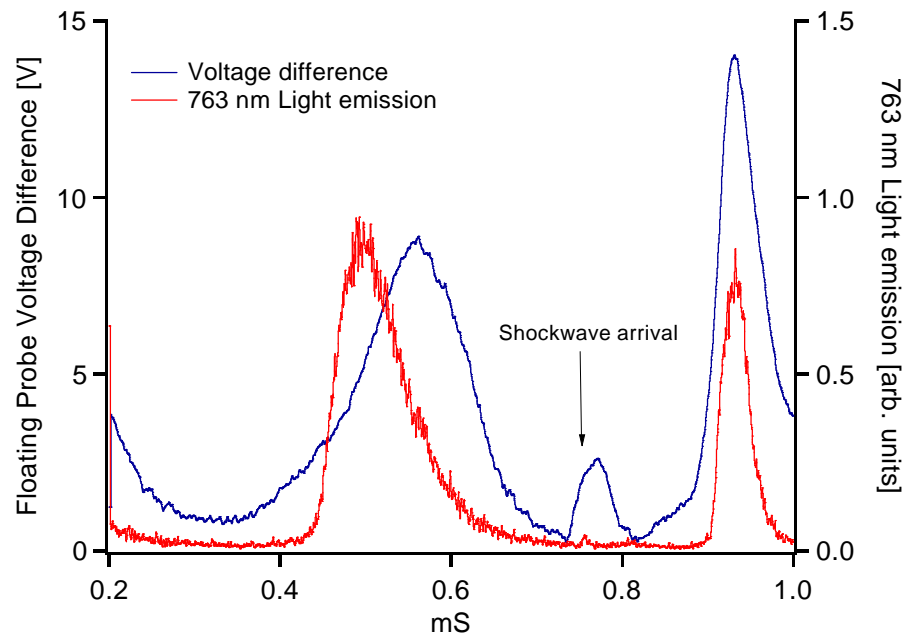nt in voltage was + 2.7 Volts with respect to the direction of the shockwave. In Figure 36, the shockwave arrived when the electron temperature was near its maximum in the ionization wave (~5.0 eV). The enhancement in voltage was + 6.6 Volts. In Figure 37, the shockwave arrived when the electron temperature was near its minimum in the ionization wave (~4.0 eV). The enhancement in voltage was + 6.6 Volts. In Figure 38, the shockwave arrives when the electron temperature was half way in between its maximum and minimum in the ionization wave (~4.5 eV). The enhancement in voltage was + 7.2 Volts. For either polarity, the double layer potential was larger for the case with the larger electron temperature. This agrees with the linear dependence of the double layer potential calculated by Jaffrin [1]. The double layer potential normalized by the electron temperature in the cathode to anode cases appears to be larger than in the anode to cathode case. The reason for this is not known, but since only four data points were collected, it is difficult to determine if this trend is real.

---

[14] The electron temperature was estimated using a numerical code, BOLSIG. The input to BOLSIG is the gas mixture and reduced electric field, *E/N*.

IV.   Analysis

The goal of this section is to describe the results found in the last section and to compare these results to the numerical calculations by Jaffrin [1] and Adamovich et al. [2].

Light Emission Explanation

The first result to explain is the increase in the light emission at the shock front. The following analysis will show that the compression of both metastable states and electrons at the shock front can account for a possible 5.3 fold jump in light emission.[15] This means that there could be an increase in light emission by 5.3 fold without needing to invoke a strong, electron-accelerating double layer, as was done by Bletzinger et al [4] and Siefert et al. [3]. As seen in Figure 28, the light emission jump ratio was always less than 4. In Equations (10) through (18), the light emission is derived before, during and after the shock front: where I = Light emission, C = constant due to solid angle of the detector with respect to the volume of excited states, n_{exc} = density of excited states ($2p_6$ for this thesis), τ_{rad} = radiative lifetime of excited state ($2p_6$ radiative lifetime to the $1s_5$ state is 36.5 nsec), k_{exc} = rate constant for electron excitation from metastable state (function of the EEDF), $v_{total\text{-}rad} = 1/\tau_{rad\ to\ 1s5\ states} + 1/\tau_{rad\ to\ non\text{-}1s5\ states} + 1/\tau_{collisional\ loss}$ = effective loss rate, n_m = $1s_5$ metastable state density and n_e = electron number density.

The light emission from the plasma near the volume of the detector is given by:

$$I = C \cdot n_{exc} / \tau_{rad} \tag{10}$$

The change in the density of excited states versus time is the production rate minus the loss rate.

---

[15] $5.3 = 2.3 \times 2.3 = (\rho_2/\rho_1)^2$ for a Mach 2 shockwave

$$\frac{dn_{exc}}{dt} = P - L = k_{exc} n_m n_e - n_{exc} \nu_{total-rad}$$

$$P = \Pr oduction = k_{exc} n_m n_e \tag{11}$$

$$L = Losses = n_{exc}/\tau_{rad} + n_{exc}/\tau_{rad-otherstates} = n_{exc} \nu_{total-rad}$$

This gives a steady state solution if we assume that the production rate equals the loss rate.

$$\frac{dn_{exc}}{dt} = 0 = k_{exc} n_m n_e - n_{exc} \nu_{total-rad}$$

$$n_{exc} = k_{exc} n_m n_e \tau_{total-rad} \tag{12}$$

Inserting the steady state solution for the excited state density into Eq (10), the steady-state light intensity is:

$$I = C \cdot n_{exc}/\tau_{rad} = C \cdot k_{exc} n_m n_e \frac{\tau_{total-rad}}{\tau_{rad}} \leq C \cdot k_{exc} n_m n_e = C \cdot P \tag{13}$$

The time-dependent solution for the light emission is:

$$\frac{dI}{dt} = \frac{\frac{dn_{exc}}{dt}}{\tau_{rad}} = \frac{(P-L)}{\tau_{rad}} \tag{14}$$

If the metastable state density doubles at the shock front, the rate of increase in the light emission would be:

$$\left.\frac{dI}{dt}\right|_{shock\ front} = k_{exc} 2n_m n_e - k_{exc} n_m n_e = k_{exc} n_m n_e \tag{15}$$

Eventually, a steady state solution is reached at the peak of the emission enhancement, given by:

$$I = 2I_{before\ shock\ front} \qquad (16)$$

If both the metastable state density and the electron number density increase at the shock front, then the rate of increase in the light emission would be:

$$\frac{dI}{dt}\bigg|_{shock\ front} = k_{exc} 2n_m 2n_e - k_{exc}n_m n_e = 3k_{exc}n_m n_e \qquad (17)$$

The peak emission intensity for this case is:

$$I = 4I_{before\ shock\ front} \qquad (18)$$

Combining the density jump ratios from Equation (1) and the light enhancement jump from Equations (16) and (18), we see that a Mach 2 shockwave is capable of a 2.3 fold light enhancement above the light emission value before the shock front if the metastable states are compressed and a 5.3 fold increase in light emission if both the electrons and metastables were compressed. This assumes that the electron energy distribution function (EEDF) does not change across the shock front[16] and this assumes that the electron number density follows the same (ρ_2 / ρ_1) dependence as the neutrals species.

Since the ratios of light emission from Figure 28 are always less than 4, we can infer that compression of metastable states and electrons is enough to explain the light emission enhancement at the shock front. The fact that the maximum compression of

[16] In partially or fully-ionized plasma, where $T_e = T_i = T_{gas}$, the electron temperature does increase across the shock front [6]. The electron temperature in the model by Adamovich et al. [2] drops from 3.6 eV to 3.2 eV across the shock front. The reason for the decrease is the decrease in E/N on the post-shock side of the shock front. Since the electron temperature near the shock front was not measured, the assumption of no change in the mean electron energy at the shock front could not be checked.

electrons, as seen in Figure 17, lags slightly behind the maximum light emission may be the reason why the light emission ratio across the shock front never reached its predicted value of 5.3. However, the other possible reason why the ratios in Figure 28 were always less than 5.3 is that the mean electron energy decreases across the shock front. Both are possible explanations and neither can be ruled out with the data collected in this thesis.

The next result to explain is the rapid decrease in light emission and metastable density (~7 μsec at Mach 2) after the light emission enhancement at the shock front (see Figure 31). The light emission is dependent on the EEDF and the metastable density. The electric field (see in Figure 24) decreases rapidly after the initial increase at the shock front. This can explain why the light emission could decay rapidly; however, a rapid decrease in the electric field can not explain a rapid loss of metastable states because their lifetime is much greater than lifetime of excited states (~36.5 nsec.) The e-folding decay time of the metastables in either the back side of an ionization wave or in the afterglow is 72 μsec for this pressure and this flow rate. As explained in Appendix A, the metastable states can be quenched by nitrogen impurities in the system. Impurity states will be compressed at the shock front; also, the gas temperature behind the shock front increases. The quenching rate of metastables by nitrogen impurities will increase with both impurity density and the thermal velocity of the metastable states. Therefore, the quenching rate across the shock front should increase proportionally to $(\rho_2 / \rho_1) \times (T_2 / T_1)^{1/2}$. This leads to a predicted e-folding decay time of the metastable states (after a Mach 2 shockwave) of 22 μsec. This predicted value is three times longer than the measured decay time of 7 μsec.

Before resolving this conflict, it will be shown that the increase in the quenching rate by $(\rho_2 / \rho_1) \times (T_2 / T_1)^{1/2}$ accurately predicts the ionization wave frequency behind the shock front. For example, when the wave frequency before the shock front was 2.56 kHz, the waves reappeared with a frequency of 4.4 kHz, 5.1 kHz, 5.6 kHz and 6.4 kHz, behind shockwaves of Mach number 1.4, 1.5, 1.7 and 1.8, respectively. This increase in ionization wave frequency can be explained by the increase in the quenching rate behind the shock front. Figure 39 shows the ratio of the wave frequency behind the shock front

to the wave frequency before the shock front. Also graphed are the density ratio, (ρ_2/ρ_1), and the density ratio times temperature ratio to the one half power, $(\rho_2/\rho_1) \times (T_2/T_1)^{1/2}$.
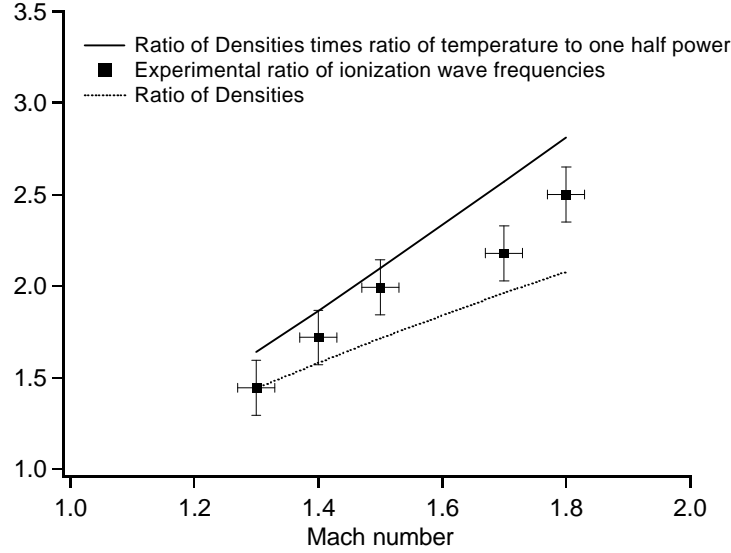
Figure 39: Ratio of Ionization Wave Frequency after Shock Front to before Shock Front

As seen in Figure 39, the actual ratio of the ionization wave frequency after the shock front to before the shock front falls in between the ratios $(\rho_2/\rho_1) \times (T_2/T_1)^{1/2}$ and (ρ_2/ρ_1). Since the lines represent maximum possible ratios, it is likely that the cause of the increased wave frequency behind the shock front is due to the increase in impurity density and the increase in velocity of the metastable states behind the shock front.

As stated above, the rapid 7 μsec decay of the metastable densities behind the shock front does not agree with the value predicted by the compression of impurities and the increase in thermal velocity. There is an alternative explanation for the rapid decrease in metastable density behind the increase at the shock front. In the laboratory reference frame, the neutral particles at the shock front acquire a directed velocity, u. In the shock reference frame, the particles are traveling towards the stationary shock front with velocity U. After the shock front, the velocity is $U - u$. In laboratory reference frame, the stationary particles acquire a velocity u behind the shock front, which is less than the shock velocity, U.
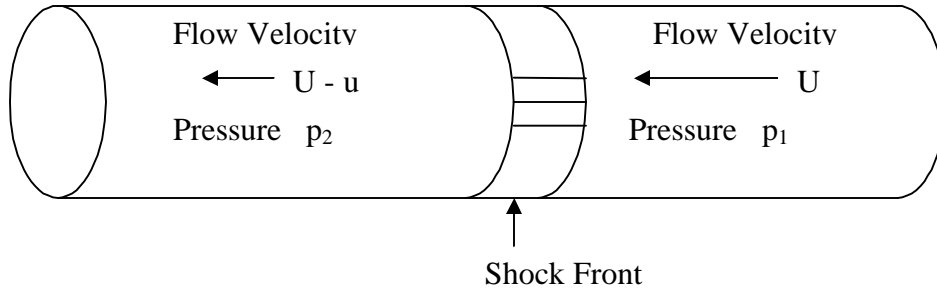
Figure 40: Diagram of Shock Front in Shockwave reference frame
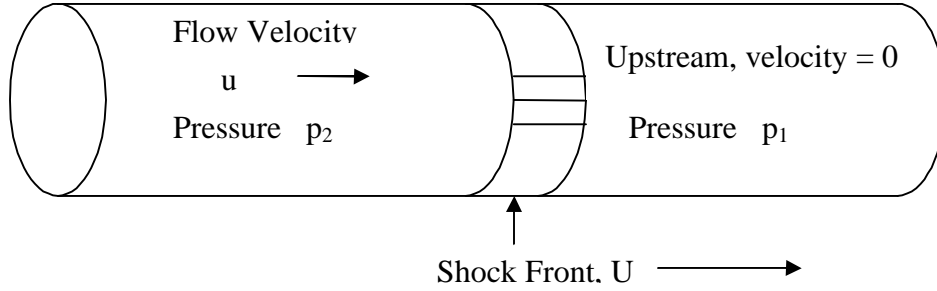
Figure 41: Diagram of Shock Front in laboratory reference frame

The velocity, u, is given by

$$\frac{u}{c_0} = 0.75 \times \left(M - \frac{1}{M} \right) \qquad , \qquad (19)$$

where c_0 is the speed of sound upstream of the shock front.

Figure 42 shows the experimentally measured e-folding decay rate of metastable states as well as the decay rate due to a) the time to travel through the width of the laser beam used to detect the particles: $\tau = 2.0$ mm $/ u$ (M) and b) the increase in quenching by a factor of $(\rho_2 / \rho_1) \times (T_2 / T_1)^{1/2}$.

55
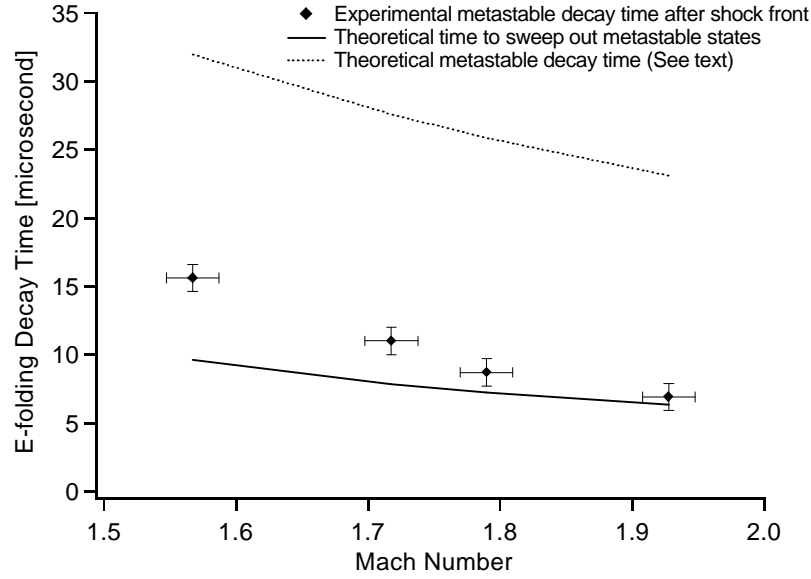
Figure 42: Decay Times of Metastable States behind Shock Front

Figure 42 shows that the sweeping out of the metastable states is the likely cause of the rapid decrease in metastable density after the shock front. The sweeping out is due to the fact that the metastable states (as well as the neutral particles) acquire a velocity, u, after the shock front in the direction of the moving shock front. This theory predicts a decay time at Mach 1.5 that is too fast, but predicts a decay time at Mach 2 that is closer to the experimental value. The increase in quenching (dotted line) by compression and increased thermal velocity does not match with the experiments results, as it did for the increase in the ionization wave frequency behind the shock front.

So far, the following have been explained: the light enhancement at the shock front, the rapid decrease in light and metastable density after this enhancement and the appearance of ionization waves with roughly twice the frequency behind the shock front. The light emission enhancement can be explained by the compression of metastable states and electrons; the rapid decrease after the enhancement can be explained by the velocity, u, all neutral species acquire behind the shock front; and the increased ionization wave frequency behind the shock front can be explained by the increase in quenching of metastable states by a factor of $(\rho_2/\rho_1) \times (T_2/T_1)^{1/2}$.

Polarization Dependence and Doubles Layers

When shockwaves are sent into discharges with ionization waves, in both the anode to cathode and cathode to anode cases, the current, *j*, was a constant. This is due to the fact that the discharge operated in a constant current mode, rather than a constant voltage mode. Still, it is quite interesting that the current remains constant with a shockwave in the middle of the discharge. The discharge current is constant even though, in the anode to cathode case, the electric field from the shock front adds to the applied electric field and, in cathode to anode case, the electric field from the shock front subtracts from the applied electric field.

At first glance, this polarization dependence resembles the polarization dependence seen by Williamson et al. [19] because in both cases the current remained constant and the electric field at the double layer added to the external electric field in one case and subtracted from the external field in the other case. However, the double layers seen in Figure 35 through Figure 38 and in Figure 18 and Figure 19 were always of positive potential. This agrees with the positive potential of the double layer predicted by Jaffrin [1] and Raizer [7]. Williamson et al. [19] found that electrons gain energy from the double layer under one polarity. At the shock front, in either polarity, the potential was positive, indicative of electrons setting up the potential, and hence losing some of their energy to the positive ions.

A rather interesting result was that the ionization waves before the shock front can be distorted only when the shockwave travels from the cathode to the anode. This is the case when the electric field of the shock front double layer subtracts from the applied electric field. In the anode to cathode case, the shockwave over takes the ionization wave, which is also traveling anode to cathode, but at subsonic speeds. The electrons, which are moving towards the anode, see the ionization wave first and then the shockwave. On the other hand, in the cathode to anode case, the shockwave and the ionization wave collide head on. The electrons, which are now heading in the same direction as the shockwave, travel through the shockwave first and then the ionization wave. This may be the reason why the ionization waves can be distorted only in the cathode to anode polarization.

V. Conclusion and Further Work

This thesis explored the interaction of neutral particle shockwaves with argon glow discharges. The density of electrons and $1s_5$ metastable states were measured across shock fronts in weakly-ionized argon to determine whether their densities could be compressed as the neutral ground state densities are compressed. Even though the electron thermal velocity can be roughly two orders of magnitude larger than the shock velocity, the data presented suggests that non-equilibrium electrons can be compressed at the shock front. The data collected with a microwave hairpin resonator showed a ratio of electron number density across a Mach 1.5 shock front of 2.1 and a ratio across a Mach 1.8 shock front of 2.7. These electron number density ratios were nearly the same in both the active discharge and in the afterglow. The corresponding neutral density ratios, given by the Rankine-Hougoniot relationship, are 1.7 and 2.0. The over-prediction of the electron compression ratio both in the steady state discharge and in the afterglow probably is due to hairpin specific effects that have been corrected yet.

Using the hairpin resonator, in combination with photo-deflection and optical fibers, established the relative location of the peak in electron density with respect to the neutral particle shock front. The location of the peak of the electron number density was displaced behind the neutral particle shock front. At Mach 1.5, the electron number density peaked 25 mm behind the shock front in the active discharge and 50 mm behind the shock front in the afterglow. This delay can not be due to the 5 mm spatial resolution of the hairpin resonator. The numerical code by Adamovich et al. [2] suggests that the electron number density should peak right at the shock front. If the slow rise in the electron number density is real, then positive ion density must also have a slow rise time. This is due to the fact that the double layer potential was always positive, i.e. electrons diffuse out in front of the positive ions. Further experiments should be conducted such that the He-Ne laser for photodeflection is aligned with the hairpin resonator. This may be difficult, but would greatly clarify the lag in the peak electron number density.

This thesis also demonstrated experimentally that metastable states can be compressed at the shock front. The measured compression ratio of metastable states in the afterglow was 25% greater than the value of the neutral species ratio for a Mach 1.8 shockwave. Data collected over a range of different Mach numbers showed the same general trend as the predicted values, but were consistently greater than predicted. This suggests that there was a systematic error in the laser frequency used in order to keep $g(\nu)$ constant across the shock front. Further experiments should be repeated using a wave-meter to determine the exact laser frequency.

Excited $2p_6$ states can not compressed at a shock front because their radiative lifetime is shorter than the time to transit though the shock front. However, the light emission from the $2p_6$ states increased across the shock front because of compression of the metastable states and electrons. Inelastic collisions between electrons and metastable states create the excited states. So, when the electrons and metastable states are compressed, there is an increase in the light emission. The light emission enhancement seen by Siefert et al. [3] and Bletzinger et al. [4] is most likely due to the compression of metastable states and electrons, and not due to an electron-accelerating double layer.

The double layer potential at the shock front was measured and compared to the double layer potential calculated by Jaffrin [1] for shockwaves in weakly ionized plasma when the electron temperature equals the gas temperature. The double layer potential measured experimentally was consistently greater than the potential calculated by Jaffrin [1] and double the value calculated by Adamovich et al. [2]. Though, within a factor of two, the experimental double layer can be predicted by using the Jaffrin theory and replacing the equilibrium temperature of the electrons by the non-equilibrium electron temperature actually encountered in glow discharges. The reason for the discrepancy between numerical calculations and experiment results may be that in the experiments the electrons have a drift velocity and in the calculations the electrons do not have a drift velocity parallel to the shock propagation. Further floating probe experiments should be conducted in the opposite polarity, the anode to cathode polarity.

Another reason for the discrepancy may be due to the fact that the weakly-ionized gas at a shock front is not technically a plasma. One of the criteria for a plasma is that

there is no net space-charge. Quasi-neutrality holds only when the electron Debye length is much smaller than the characteristic length at which there is a gradient in the electron number density. This criterion breaks down at a shock front in glow discharges because the Debye length is comparable to the shock thickness. The ambipolar diffusion of electrons assumed by Jaffrin [1] breaks down when the Debye length is comparable to the characteristic length of diffusion.

Regions where quasi-neutrality breaks down are scientifically interesting because the diffusion of electrons is neither ambipolar diffusion nor free diffusion. Further research should be directed at determining both the ion and electron number densities as the shock wave passes to an accuracy of ~0.5 mm. Unfortunately, there is currently no way to measure the positive ion density with such resolution. The electron number density was measured by a microwave hairpin resonator, but only under limited discharge conditions and with an axial resolution of 5 mm. An important parameter not measured in these experiments was the electron temperature. If the electron temperature were known, then it may be possible to determine conclusively whether electrons gain energy in the double layer at the shock front.

It may also be worthwhile to repeat these experiments in neon rather than argon. Argon was chosen because a) its weight is comparable to nitrogen b) there is diode laser available to measure its metastable state densities and c) it is cheap to purchase. But since this work raised some very interesting basic questions (such as how stable are glow discharges to shockwaves? And what is the magnitude of the double layer at the shock front in non-equilibrium plasma?), it may be worthwhile to replicate these experiments with neon. Experiments in helium may be hard because it is difficult to generate shockwaves in a medium with such a large speed of sound.

A major undertaking would be to measure the time-dependent electric field at the shock front using Stark spectroscopy. One could work in helium and measure the electric field at the shock front by measuring a shift in the helium energy levels due to the electric field of the double layer. The electric field data should, in theory, agree with the electric fields seen in Figure 2.

Appendix A: Ionization Waves

If a voltage is applied across two cylindrical electrodes separated by cylindrical glass walls, the solution of the electron number density in the discharge tube should not depend on the angle theta, i.e. there is azimuthal symmetry about the z-axis (z-axis is the line through the discharge that connects the two electrodes.) Also, the solution should not, if the mass of the two charged species were equal, depend on the position along the z-axis. However, this symmetry along the z-axis is broken because there is a difference in mass between the negatively charged species and the positive charged species. This partially explains why the discharge variables (such as light emission or electron number density) are a function of position along the z-axis. In many discharges, however, there is a region called the positive column for which the light emission, electron number density, etc. are not a function of position. In the positive column, at least, there is symmetry along the z-axis, i.e. one can move along the z-axis and there is no change in the values of the discharges variables. On the other hand, there exists a whole range of discharges for which this symmetry along the z-axis in the positive column does not hold. In these discharges, there exists either standing or moving waves.

Review of Previous Studies

As mentioned in the introduction, there exist different types of ionization waves. Some are due to recombination instabilities; others are due to attachments instabilities. Currently, there are two main approaches to studying the ionization waves seen in this thesis. The two approaches may be related, but the connection is not apparent. The first approach focuses on the non-local behavior of the electron energy distribution function (EEDF) and the other focuses on a series of coupled nonlinear equations. The nonlinearity in this system stems from the presence of metastable states.

The first approach to ionization waves is presented by Golubovskii et al. [36]. They numerically solved the Boltzmann kinetic equation, including elastic and inelastic collisions as well as spatial gradients along the electric field. The presence of phase shifts

between ionization rate and electron number density caused the propagation of ionization waves. Moving potential structures travel through the discharge with a voltage exactly equal to the voltage difference between the lowest lying metastable state and the ground electronic state. Golubovskii et al. [37] calculated the phase shifts between ionization rate and electron number density, and they showed that unexpectedly large phase shifts between fields and rates of excitation and ionization can occur. In their models, the EEDF is not being formed by the local field in each phase of the striation, but the whole potential profile. At pressures around 2 Torr, step-wise ionization dominated.

The other approach stems from work at the University of Miami, starting with H.S. Robertson [16] and ending with Huerta et al. [38]. Robertson demonstrated in a numerical model that two-step ionization of metastables leads to an instability when the current is below a certain value. This model confirms what is known experimentally as the Pupp upper limit for striations in noble gases. Also, if there are no metastable states or only a small number of them, then the plasma was found to be stable. This coincides with the fact that there is a lower limit to the current, i.e. striations do not appear below a certain threshold of current (see Figure 43). Huerta et al. [38] reported the formation of orderly, steady, spatial structures (like balls of fire) in rf-heated plasmas that have metastable states. The structures were described as an instability of the reaction-diffusion equations for the plasma species. Huerta et al. [38] used the methods of bifurcation theory to calculate the non-uniform states that bifurcate from the unstable steady state. In their model, a term in the electron source function with a $n_m n_e^2$ dependence was the crucial term that allowed the instability to develop. This term is caused by the "pseudo-metastable" character of the $1s_2$ and $1s_4$ states found in Ar and Ne. The $n_m n_e^2$ term in the source function for electrons is due to three-step ionization, i.e. excitation of the $1s_5$ or $1s_3$ metastable, followed by collisional quenching to the $1s_2$ or $1s_4$ radiative states, finally followed by electron impact of the radiative state to the positive ion level. This model is an expansion of the previous model by Robertson [16], and therefore explains both the experimentally determined current limits and the chaotic nature of ionization waves.

The similarity between the two approaches seems to be two-step ionization from the metastable state. The following are some the experimentally-determined results for

ionization waves. First, for noble gases at these pressures and currents, the ionization wave travels from the anode to cathode. Second, the circuit parameters, such as the ballast resistance, do not define the oscillation frequency of the discharge [13]. Third, the ionization waves are an example of self-organization. Striated medium is normally associated with nonlinear feedback. Self-organization can also appear as chaos. This occurs when multiple ionization wave frequencies are competing in the discharge. This phenomenon has been well documented [39]. Atipo et al. [40] studied neon glow discharges and measured the optical emission along the discharge length as a function of time. They charted the transition of the wave from being period-1 to quasi-periodic to chaotic and finally to fully turbulent. They also include graphs of the unstable orbits, Lyanpunov constants and the correlation dimension of the ionization waves.

Experimental Results

The following results are included to show the chaotic nature of ionization waves. Figure 43 shows that there can be a sharp increase in the wave frequency.
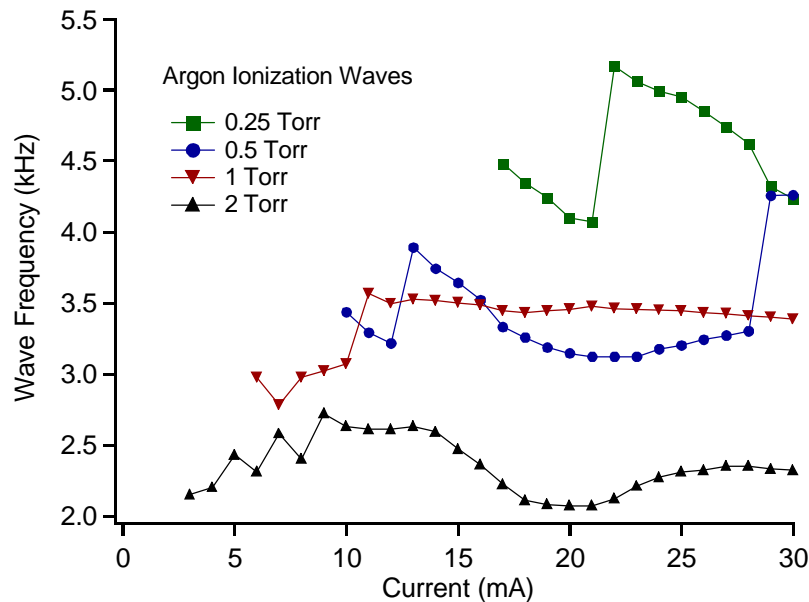

Figure 43 : Ionization Wave Frequency versus Current

The sharp increases in frequency in Figure 43 are bifurcations and the in-between currents have waves that are chaotic. One can also see how the lower limit of current is a function of pressure. For example, there are no ionizations below 3 mA at 2 Torr, below 6 mA at 1 Torr, below 10 mA at 0.5 Torr and below 17 mA at 0.25 Torr.

Figure 44 (next page) shows Fast Fourier Transforms (FFTs) of the light emission as the discharge current is slowly increased through a bifurcation. The sharp transitions seen in Figure 43 are not smooth. In the transition region, multiple frequencies are competing, and the discharge becomes chaotic. Here, chaos means that there is at least one positive Lyapunov exponent, i.e. the competing wave frequencies do not dampen out during the bifurcation.
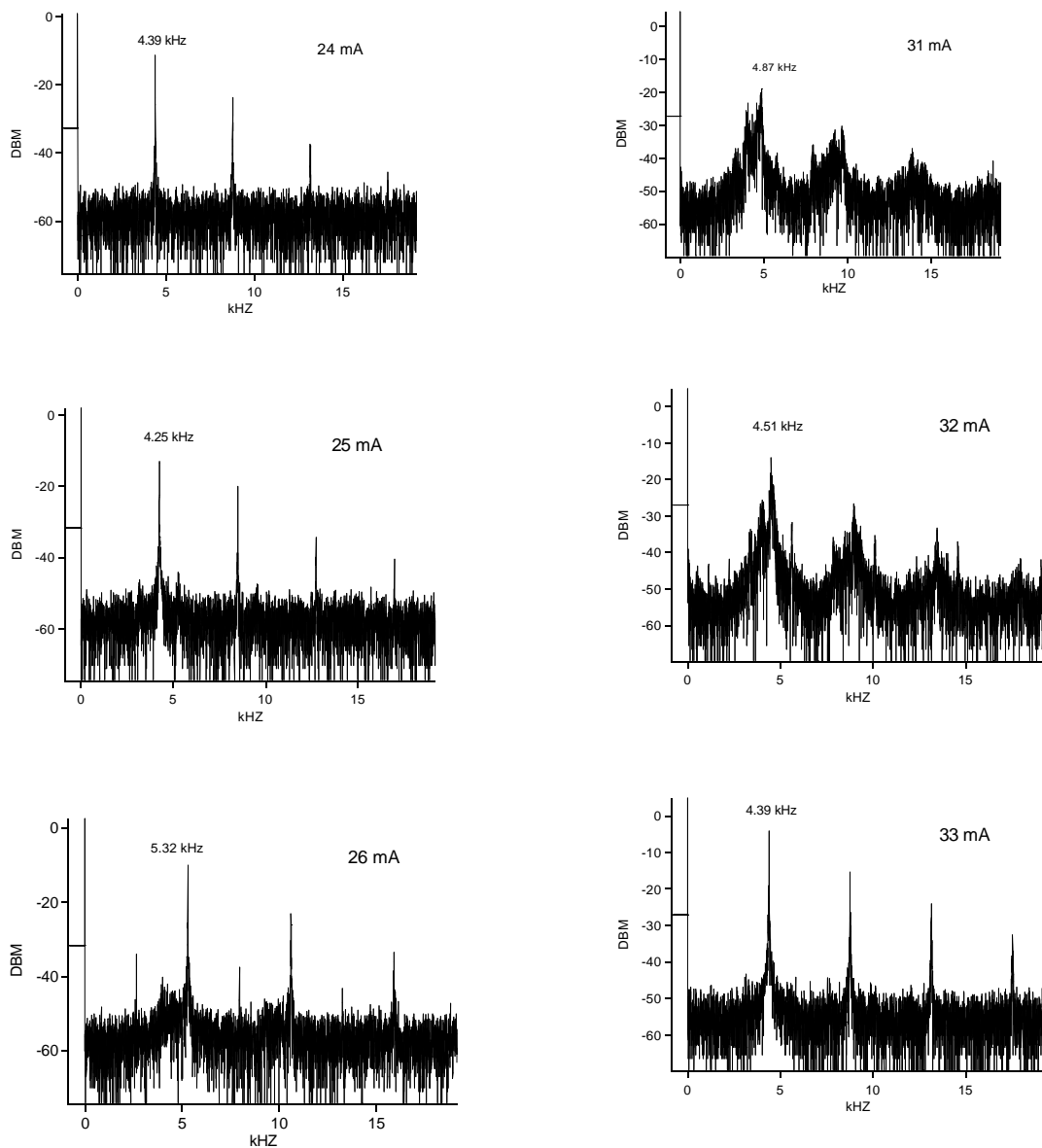
Figure 44: FFTs of Light Emission for Increasing Current through a Bifurcation

Figure 44, the FFTs at 24, 25 and 33 mA show that one principal frequency dominates. The higher frequencies are multiples of the principal frequency due to the fact that the ionization waves are not sinusoidal. The FFT at 26 mA shows a period doubling. The FFTs for 31 mA and 32 mA show that multiple principal frequencies are competing with each other. By 33 mA, the discharge once again has one principal frequency.

Another interesting feature of the ionization studied was that the wave frequency depended on the air impurity level. Figure 45 shows the ionization wave frequency and the decay time of metastable states in the afterglow as a function of the flow of argon through the discharge tube.
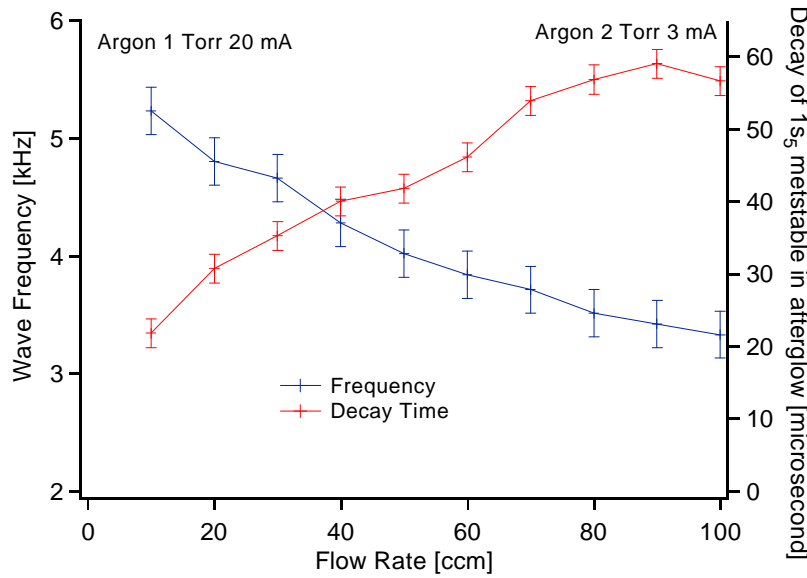

Figure 45: Ionization Wave Frequency and Decay Time of $1s_5$ Metastables in Afterglow versus Flow Rate

The wave frequencies were collect in an argon glow discharge at 1 Torr 20 mA. The decay time data was collected in the afterglow of a 2 Torr 3 mA discharge. As discussed in the experimental results section, the metastable states can be quenched by nitrogen impurities and electrons. For this set of data, the discharge current was kept constant while varying the impurity level by changing the flow rate of argon through the

66

discharge. The impurity level of the discharge is proportional to the leak-in rate (a constant) divided by the flow rate.

The left axis of Figure 45 shows how the flow rate of argon through the discharge causes a change in the wave frequency. A higher flow rate corresponds to a lower level of impurities in the discharge. The current was kept constant, so the electron number density was also approximately constant. The wave frequency increased as the flow rate decreases, i.e. as the impurity level in the discharge increases. The right axis shows that the lifetime of the $1s_5$ metastable state in the afterglow decreased with increasing impurity level. The frequency of the ionization waves can only increase and the lifetime in the afterglow can only decrease if the dominate mechanism for quenching of the metatstable state were collisions with nitrogen impurities.

This appendix has shown that metastable states are the cause of the ionization wave and that their lifetime is determined by the density of nitrogen impurities. The chaos seen in these discharges appears to be caused by two-step or three-step ionization. The frequency of these ionization waves, under these discharge conditions, was not determined by the ambipolar diffusion time of the charged species, but rather was determined by the quenching rate of the metastable states.

Stability Analysis

This appendix concludes with an analysis of the stability of glow discharges under three different conditions: 1) recombination dominated; 2) ambipolar diffusion dominated; and 3) two-step ionization dominated. This is done in order to show that steady-state solutions are not stable in discharges where two-step ionization dominates. The first case analyzed is a discharge whose charged species are made in electron ionization collisions with ground states and are lost in 3-body recombination. (e = electron, X = ground state, I = positive ion, k_{ion} = ionization rate constant, k_{rec} = recombination rate constant and ω is the eigenvalue of the perturbation.)

The reaction equations for this case are:

$$e + X \xrightarrow{k_{ion}} I + 2e$$
$$e + I + X \xrightarrow{k_{rec}} 2X \qquad (20)$$

These equations lead to a differential equation for the density of charged particles.

$$\frac{\partial n_e}{\partial t} = \frac{\partial n_i}{\partial t} = k_{ion} n_e n_x - k_{rec} n_e^2 n_x \qquad (21)$$

When the production equals the losses, the steady-state solution for the charged particle density is:

$$\frac{\partial n_e}{\partial t} = 0 = n_e n_x \left(k_{ion} - k_{rec} n_e \right)$$
$$n_e^0 = \frac{k_{ion}}{k_{rec}} \qquad (22)$$

We now add a perturbation to the steady state density.

$$n_e = n_e^0 + \delta n_e e^{\omega t}$$
$$\omega = -k_{ion} n_x \qquad (23)$$

There exists one eigenvalue and it has a negative value. Therefore, any perturbations get damped out. This makes sense because an increase in electron number density increases the ionization rate linearly but increases the recombination quadraticly.

The second case analyzed is a discharge whose charged species are made in electron ionization collisions with ground states and are lost in ambipolar diffusion to the wall. (v_{amb} = ambipolar diffusion frequency)

The reaction equations for this case are:

$$e + X \xrightarrow{k_{ion}} X + 2e$$
$$e + I \xrightarrow{v_{amb}} X \qquad (24)$$

These equations lead to a differential equation for the density of charged particles.

$$\frac{\partial n_e}{\partial t} = \frac{\partial n_i}{\partial t} = k_{ion} n_e n_x - \nu_{amb} n_e \qquad (25)$$

When the production equals the losses, the steady-state solution for the charged particle density is:

$$\frac{\partial n_e}{\partial t} = 0 = n_e \left(k_{ion} n_x - \nu_{amb} \right)$$
$$n_e^{\ 0} \; constrained \; by \; k_{ion} n_x = \nu_{amb} \qquad (26)$$

We now add a perturbation to the steady state density.

$$n_e = n_e^{\ 0} + \delta n_e e^{\omega t}$$
$$\omega = 0 \qquad (27)$$

Here, we have the case where any value of n_e is allowed in the steady state solution, as long as the production equals the losses. Since there is only one eigenvalue and its value is zero, a perturbation to the steady state is stable, but only conditionally stable. Perturbations do not grow nor dampen. Perturbations can grow if second order effects are included, such as heating of the gas.

The third case analyzed is a discharge whose charged species are made in step-wise ionization from the metastable state and are lost by ambipolar diffusion to the wall. The metastable state is created by electron excitation from the ground state and is lost by step-wise ionization and collisions with nitrogen impurities. (M = metastable state density, IMP = impurity state density, $k_{2\text{-}step}$ = two-step ionization rate constant, k_m = rate constant for excitation of the ground state to the metastable state and ν_{quench} = frequency of quenching metastables states by impurity states.)

The reaction equations for this case are:

$$e + X \xrightarrow{\;k_m\;} e + M$$

$$e + I \xrightarrow{\;\nu_{amb}\;} X$$

$$e + M \xrightarrow{\;k_{2step}\;} I + 2e \tag{28}$$

$$M + IMP \xrightarrow{\;\nu_{quench}\;} X + IMP$$

These equations lead to differential equations for the density of charged particle and density of metastable states.

$$\frac{\partial n_e}{\partial t} = \frac{\partial n_i}{\partial t} = k_{2step} n_e n_m - \nu_{amb} n_e$$

$$\frac{\partial n_m}{\partial t} = k_m n_e n_x - k_{2step} n_e n_m - \nu_{quench} n_m \tag{29}$$

When the production equals the losses, the steady-state solution for the charged particle density and metastable density are:

$$\frac{\partial n_e}{\partial t} = 0 = n_e \left(k_{2step} n_m - \nu_{amb} \right)$$

$$n_m^{\;0} = \frac{\nu_{amb}}{k_{2step}} \tag{30}$$

$$n_e^{\;0} = \frac{\nu_{amb} \nu_{quench}}{k_{2step} \left(k_m n_x - \nu_{amb} \right)}$$

We now add a perturbation to the steady state solutions.

$$n_e = n_e^{\;0} + \delta n_e e^{\omega t}$$

$$n_m = n_m^{\;0} + \delta n_m e^{\omega t} \tag{31}$$

$$\omega^2 + \omega \left(\frac{k_m n_x \nu_{quench}}{k_m n_x - \nu_{amb}} \right) - \nu_{amb} \nu_{quench} = 0$$

In this case, there are two values of omega. One of those values will always be negative and the other will always be positive. Since the solution has one positive solution, small perturbations will always grow. Therefore, a stable solution to n_e and n_m is not possible. This highlights the main features of why two-step ionization in a noble gas discharge leads to an instability. However, this model breaks down when the quenching rate is much larger than the excitation rate because there is a transition from predominantly two-step ionization to predominantly direct ionization.

This section includes more graphs from the 30 mA, 2 Torr and Mach 2 data in the results section. The following three graphs are included to show what happens if the shock front arrives at different phases of the ionization wave. The shockwaves traveled from the anode to the cathode. In Figure 48, note how the shockwave arrives on the front side of the ionization wave (Phase 86 degrees) and on the back side of the ionization wave (Phase 174 degrees), but that the post-shockwave ionization wave starts up at the same time. Also note that the time basis in Figure 48 is not the same as the time basis in Figure 46 and Figure 47.
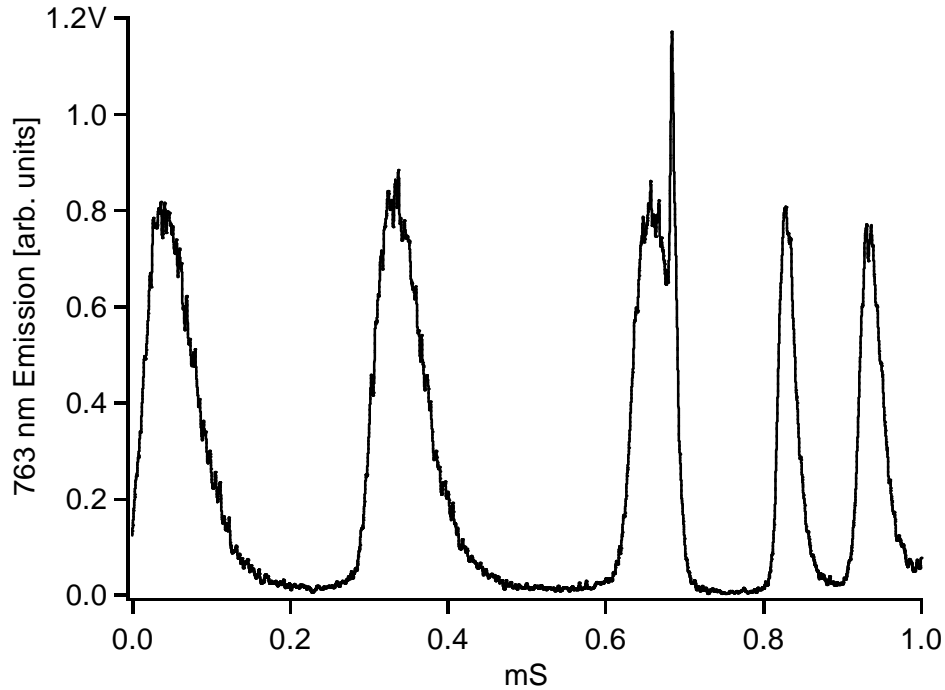

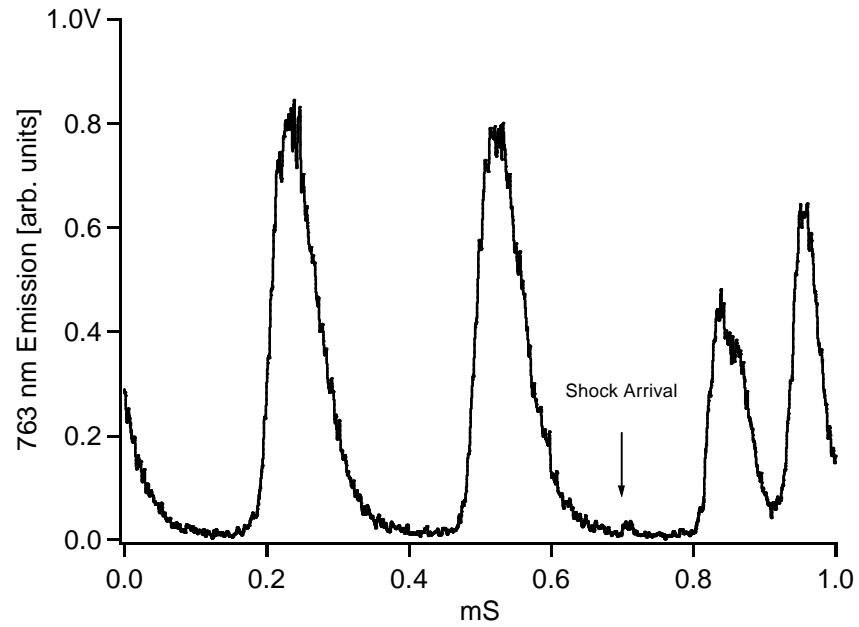Figure 46: Shockwave arrives at a Phase of 170 degrees

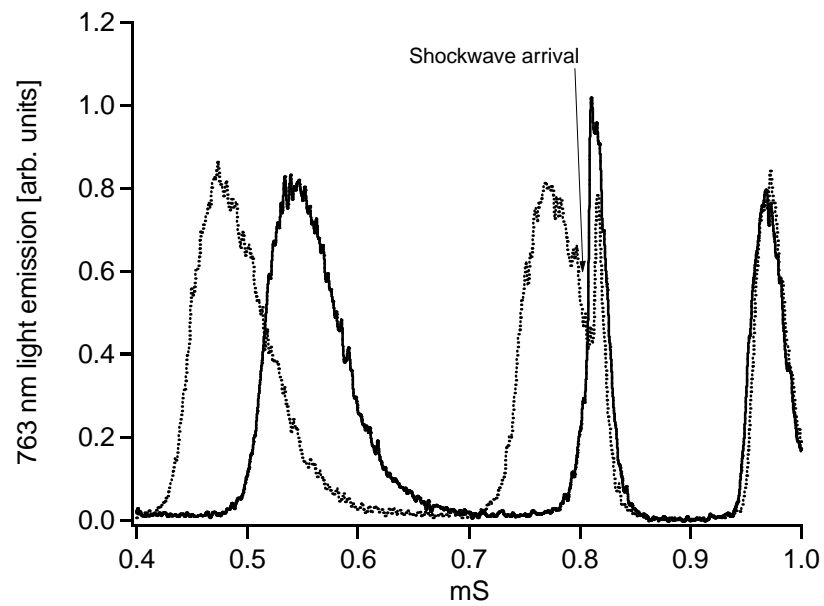Figure 47: Shockwave arrives at a Phase of 326 degrees

Figure 48: Shockwave arrives at a Phase of 86 degrees (full curve) and 174 degrees (dotted curve)

These figures show, once again, that the light emission enhancement at the shock front is proportional to the light emission before the shock front, i.e. the jump in emission is larger when there are is more emission to start with. It is also fascinating that the ionization waves behind the shock front start up at the same time even though the shockwave arrives at a different phase of the ionization wave. In Figure 46, it is clear that the ionization wave frequency behind the shock front is greater then the ionization wave frequency before the shock front. This data appears as one of the data points in Figure 39.

Bibliography

[1]   Jaffrin, M., *Phys. Fluids*, **8**, 606 (1965).

[2]   Adamovich, I.V., Subramanium, V.V., Rich, J.W., and Macheret, S.O., *AIAA Journal*, **36**, 816 (1998).

[3]   Siefert, N., Ganguly, B.N., Bletzinger, P., *Phys. Rev. E*, **72**, 066402 (2005).

[4]   Bletzinger, P., Ganguly, B.N. and Garscadden, A., *Phys. Rev. E*, **67**, 047401 (2003).

[5]   Greenberg. O.W., Sen, H.K., Treve, Y.M., *Phys. Fluids.*, **3**, 379 (1960).

[6]   Liberman, M.A. and Velikovich. A.L., "Physics of Shock Waves in Gases and Plasmas." Springer-Verlag, New York, 1986 pp 91 – 110.

[7]   Zel'dovich, Y.B. and Raizer, Y.P., "Physics of Shock Waves and High-Temperature Hydrodynamic Phenomena Vol II." Academic Press New York, 1967 pp. 515-526.

[8]   Gerber, R.A. and Gerado, J.B., *Phys. Rev. A*, **7**, 781 (1973).

[9]   Phelps, A.V., *J. Res. Natl. Inst. Stand. Technol.*, **95**, 407 (1990).

[10]   Persson, K.B., *Phys. Fluids*, **5**, 1625 (1962).

[11]   Bletzinger, P., Ganguly, B.N., and Garscadden, A., *IEEE Trans. Plasma Sci.*, **33**, 342 (2005).

[12]   Perarek, L., *Soviet Physics Uspekhi*, **11**, 188 (1968).

[13]   Olsen, N.L. and Cooper, A.W., "Moving Striations," *Advances in Electronics and Electron Phyics.*, Vol 24, 1968.

[14]   Garscadden, A. "Ionization Waves in Glow Discharges" in *Gaseous Electronics Vol I. Academic Press*, 1978.

[15]   Raizer, Y.P.. "Gas Discharge Physics," Springer-Verlag, Berlin, 1991, Ch 9, 214-266.

[16]   Robertson, H.S., *Phys. Rev,*, **105**, 368 (1957).

[17]   Coakley, P. and Hershkowitz, N., *Phys. Fluids.*, **22**, 1171, (1979).

[18] Chiu, G.S. and Cohen, S.A., *Phys. Rev. Lett.*, **76**, 1248, (1996).

[19] Williamson, J.M. and Ganguly, B.N., *Phys. Rev. E*, **64**, 036403 (2001).

[20] Hershkowitz, N., *Space Science Reviews,* **41,** 351 (1985).

[21] Lysak, R.L. and Andre, M., *Phys. & Chem. of the Earth: Part C*, **26**, 3 (2001).

[22] Cohen, S. A., Siefert, N.S., Stange, S., Boivin, R.F., Scime, E.E. and Levinton, F.M., *Phys. Plasmas*, **10**, 2593 (2003).

[23] Ishiguro, S., Kamimura, T., and Sato, T., *Phys. Fluids*, **28**, 2100 (1985).

[24] Maciel, H.S. and Allen, J.E., *J. Plasma Phys*. **42**, 321 (1989).

[25] Kiffer, J.H., and Lutz, R.W., *J. Chem. Phys.*, **44**, 658 (1966).

[26] Raizer, Y.P., *Gas Discharge Physics*, (Springer-Verlag, Berlin, 1991), pp. 200.

[27] Stenzel, R.L., *Rev. Sci. Instrum.*, **47**, 603 (1976).

[28] Piejak, R.B., Godyak, V. A., Garner, R., and Alexandrovich, B.M., *J. Appl. Phys.* **95**, 3785 (2004).

[29] Herald, M.A. and Wharton, C.B., "Plasma Diagnostics with Microwaves," (John Wiley & Sons Inc., New York, 1965) pp. 6, 63-65.

[30] Golubovskii, Y.B., Maiorov, V.A., Kozakov, R. V., Solyman, S., Stockhausen, G., and Wilke, C., *J. Phys. D*, **34**, 1963 (2001).

[31] Penache, C., Miclea, M., Brauning-Demian, A., Hohn, O., Schossler, S., Jahnke, T., Niemax, K., and Schmidt-Bocking, H. *Plasma Sources Sci. & Technol.*, **11**, 476 (2002).

[32] Wiese, W.L., Smith, M.W., Miles, B.M. *Atomic Transition Probabilities Volume II*, NSRDS-NBS 22, 1969.

[33] Dasgupta, A., Blaha, M. and Giuliani, J. L., *Phys. Rev. A*, **61**, 012703 (1999).

[34] Velazco, J.E., Kolts, J.H., and Setser, D.W.. *J.Chem. Phys.* **69**, 4357 (1978).

[35] SIGLO Homepage. www.siglo-kinema.com/bolsig.htm

[36] Golubovskii, Y.B., Kozakov, R.V., Maiorov, V.A., Behnke, J., Behnke, J.F., *Phys. Rev. E*, **62**, 2707 (2000).

[37] Golubovskii, Y.B., Maiorov, V.A., Porokhova, I.A., and Behnke, J., *J. Phys. D*, **32**, 1391 (1999).

[38] Huerta, M. A., and Magnan, J. F., *Phys. Rev. A*, **26**, 539 (1982).

[39] Koepe, M.E., Klinger, T., Seddighi, F. and Piel, A., *Phys. Plasmas*, **3**, 4421 (1996).

[40] Atipo, A., Bonhomme, G. and Pierre, T., *Eur. Phys. J. D*, **19**, 79 (2002).

Vita

       Lieutenant Nicholas S. Siefert graduated from Poway High School in San Diego, California. He entered undergraduate studies at Princeton University where he graduated with honors with a Bachelor of Science and Engineering in Mechanical & Aerospace Engineering. While at Princeton, he first was introduced to the topic of shockwave/plasma interactions under guidance of Drs. Richard Miles and Sergey Macheret. He was commissioned through the AFROTC Detachment 485.

       His first assignment was to Wright Patterson, AFB, where he was first assigned to the F-16 System Program Office and then assigned to the Propulsion Directorate of the Air Force Research Labs. While at the research labs, he worked with Drs. Biswa Ganguly and Peter Bletzinger in the area of shockwave/plasma interactions. During this time, he attended the Air Force Institute of Technology as a part-time Master's student with funding from the Dayton Area Graduate Studies Institute.

1. REPORT DATE *(DD-MM-YYYY)* 03-23-2006	2. REPORT TYPE **Master's Thesis**	3. DATES COVERED *(From – To)* Jun 2005 – Mar 2006

4. TITLE AND SUBTITLE Shockwave Interactions with Argon Glow Discharges	5a. CONTRACT NUMBER
	5b. GRANT NUMBER
	5c. PROGRAM ELEMENT NUMBER
6. AUTHOR(S) Siefert, Nicholas, S., Lieutenant, USAF	5d. PROJECT NUMBER
	5e. TASK NUMBER
	5f. WORK UNIT NUMBER

7. PERFORMING ORGANIZATION NAMES(S) AND ADDRESS(S) Air Force Institute of Technology Graduate School of Engineering and Management (AFIT/EN) 2950 Hobson Way WPAFB OH 45433-7765	8. PERFORMING ORGANIZATION REPORT NUMBER AFIT/GAP/ENP/06-18
9. SPONSORING/MONITORING AGENCY NAME(S) AND ADDRESS(ES) N/A	10. SPONSOR/MONITOR'S ACRONYM(S)
	11. SPONSOR/MONITOR'S REPORT NUMBER(S)

12. DISTRIBUTION/AVAILABILITY STATEMENT APPROVED FOR PUBLIC RELEASE; DISTRIBUTION UNLIMITED

13. SUPPLEMENTARY NOTES

14. ABSTRACT

The purpose of this research was study shockwave interactions with argon glow discharges. Specifically, this thesis sought to answer whether it is possible to compress nonequilibrium electrons at the shock wave. The results in the thesis found that both equilibrium and nonequilibrium electrons could be compressed at the shock front. The double layer a t the shock front, normalized by electron temperature, matched the calculated values for the double layer within a factor or two in all cases. The results also demonstrate that excited metastable states can be compressed at the shock front, as well.

The culmination of this effort was to show that electrons can be compressed and that the double layer is orientated such that electrons do not gain energy from the shock front. This was done in order to help explain results by previous researchers in the area of plasma-shockwave interactions.

15. SUBJECT TERMS Shock wave, glow discharge, microwave interferometry, diode laser

16. SECURITY CLASSIFICATION OF:			17. LIMITATION OF ABSTRACT	18. NUMBER OF PAGES	19a. NAME OF RESPONSIBLE PERSON William F. Bailey, (ENP)
REPORT U	ABSTRACT U	c. THIS PAGE U	UU	92	19b. TELEPHONE NUMBER *(Include area code)* (937) 785-3636, ext 4501; e-mail: William.Bailey@afit.edu

Standard Form 298 (Rev: 8-98)
Prescribed by ANSI Std. Z39-18